Assessment of Mechanical, Thermal Insulation and Water Sorption Properties of Natural Fiber-
Cement Composites

by

Kareem Abdelghany

A thesis submitted in partial fulfillment of the requirements for the degree of

Master of Science

Department of Renewable Resources
University of Alberta

Abstract

The growth of awareness about the environmental issues caused by the construction industry has fueled innovation in sustainable building practices in recent years. Of particular concern is the need for solutions to reduce the high carbon footprint of current building materials such as cement and concrete. A potential remedy to the adverse environmental effects of the construction industry is the replacement of non-renewable materials with a natural and easily renewable counterpart. This study investigates the effects of fiber type, fiber volume fraction, and fiber size on the compression, flexural, thermal insulation and water absorption properties of natural fiber cement composites. The fibers used were obtained from Alberta based crops: wheat straw and hemp hurd. These fibers were each sieved and characterized in two size categories, coarse and fine, and added to the cement at 3 volume fractions: 5%, 10%, and 15%. The results indicate that the addition of fibers to cement decrease the compression strength, increase the flexural strength, increase the thermal resistivity, and increase the saturation moisture content of the composite compared to the control (unreinforced cement). In addition, a moisture sorption model based on Fick's law showed reasonable fit to the experimental data. Overall, this study demonstrated that cements reinforced with natural fibers offer improved flexural (crack resistance) and insulating properties compared to unreinforced cement which may be advantageous in a number of building product applications (e.g. architectural or non-structural components). However, these natural fiber composites also had reduced compressive strengths, and were more susceptible to moisture uptake. These characteristics may affect the usage of these materials in main structural components, and may also require proper protection from moisture in outdoor applications.

Acknowledgement

Table of Contents

List of Tables

List of Figures

1.0 Introduction

The growth of awareness about the high levels of pollution produced by the construction industry has fueled innovation in sustainable building practices in recent years [1]. In light of these challenges, there has been recent interest in sustainable materials and design for the building construction sector. There has been a steady increase in the construction of more sustainable buildings in Canada over the past 12 years based on LEED standards [2].

Building materials play a major role in the sustainability of a project. Materials selection not only affects the physical performance and aesthetics of buildings but also their energy consumption, carbon footprint, life cycle and cost of production. Cements are the most common engineering materials used today with a global production of more than 4.4 billion annually [3]. Of this market, the most common type of cement used is "Portland Cement" which is the basic ingredient of most concrete and mortar applications. Unfortunately, the cement industry is estimated to be responsible for 5% of all anthropogenic carbon dioxide production globally [4]. This CO_2 is emitted from several steps in the cement manufacturing process including the calcination of limestone, the combustion of fuels in the kiln, and energy generation [4-5].

A potential solution to this adverse environmental effect is the replacement of cement with a natural and readily renewable component such as natural fibers (NF) made from lingo-cellulosic biomass. Western Canada has an abundance of available biomass both from agricultural and forestry feedstocks. From the agriculture sector alone, it is estimated that 37 million tonnes of straw from wheat, barley, oats and flax are produced annually in the provinces of Alberta, Saskatchewan and Manitoba [6]. While a portion of this straw is required to maintain

an important carbon source for soil maintenance, the excess from this production represents an underutilized pool of natural and easily accessible raw material for commercial use. Another lignocellulosic fiber that is an agricultural fiber is hemp hurd which is the woody inner core of the hemp stalk (*Cannabis sativa*). Industrial hemp production is seeing increased growth in Canada over the past number or years due to its use in both food and non-food (cellulosic fiber) applications [7]. Furthermore, industrial hemp is well suited for Canadian climatic conditions, and can produce significant bio-mass yields (as an example, in the province of Quebec, the average dry hemp biomass yield is 3.2 t/ha per harvest) [8]. With uses limited to animal bedding and mulch, hemp hurd represents another underutilized biomass pool. A cement product that incorporates these agricultural fibers will not only provide a sustainable and more environmentally friendly alternative to conventional building materials, but could potentially provide farmers with a value-added revenue stream.

This objective of the current study is to investigate the potential use of two natural fibers, wheat straw and hemp hurd, as a feedstock to produce cement-based composites. The overall goal of the study is to produce various cement composite options and asses their property limits for use in sustainable building construction. The study focuses on the effects of fiber type (hemp hurd and wheat straw), particle size (fine and coarse), and fiber volume fraction (5%, 10%, 15%) on the compression strength, flexural strength, thermal insulation properties, and water sorption properties of the final composite. The intent is to provide designers and engineers with new material options and necessary performance data which can be used to improve the sustainability of conventional building designs.

2.0 Literature Review

2.1 Introduction to Cement Based Composite Materials

A composite material is a material that is compromised of two or more distinct constituents that when combined produce a new material with improved performance compared to its individual parts [9]. Composites differ from other types of materials since their components' act as one when combined, however, they typically remain as distinct phases (i.e. do not fully mix or dissolve). Generally, composites have a matrix phase and a reinforcement phase.

Cement composites are composite materials that are composed of a particulate and/or fiber phase bound within as cement matrix phase. Concrete is a common cement composite made with cement, sand, aggregate and other components. Cement is generally a brittle material that is designed to withstand loading mainly in compression, but can be prone to cracking. Fibers are often added in cements and concrete to alleviate the material's poor fracture toughness (low resistance to cracking) and to improve durability [10]. Fiber characteristics that affect the bonding between the fiber and the matrix include the shape, surface roughness, and the surface chemistry of the fiber.

Fiber reinforced concrete has also been used in the construction and repairs of dams, bridge decks, mines, tunnels, canals and reservoirs [11]. These applications rely on the fiber to enhance the toughness and structural integrity of the concrete. Glass fiber, polypropylene, nylon, steel and natural fibers are some of the most common fibers used in fiber reinforced concrete. While a vast majority of fibers used are manufactured using synthetic materials (petro-chemical

based polymers, metals and ceramics), there is a growing interest in the use of renewable, natural fibers in these applications.

Natural fibers have been widely used throughout history in building construction, either on its own or as a reinforcement for other materials. In ancient civilizations with limited access to wood and timber, local resources such as reeds and straws were often used as building materials. As an example, the ancient Egyptians manufactured mud bricks by using locally available natural materials harvested from the environment around them [12]. Mud bricks were manufactured by mixing alluvial Nile sediment with desert sand and straw. This produced a malleable mixture which was pressed into moulds, as was either sun or kiln dried.

Using natural fibers as a reinforcement for cements and concrete, relative to synthetic fibers, has many advantages. These include their low cost, high toughness, high specific strength, low density, and ease of renewability [13]. The mechanical performance of lignocellulosic fiber cement composites has been investigated relative to different fiber types, fiber sizes, and fiber volume fractions. The influence of these factors on the compression strength, flexural strength, water absorption, and thermal insulation of these composites are of interest as these are the main factors that dictate the usability of these materials in a building construction application. A comprehensive categorization and summary of previous natural fiber cement and concrete studies is provided in Table 1.1. This table summarizes the specific materials investigated and provides a checklist of which characterization tests that were performed in the studies. This table will be an invaluable resource for those looking to study and develop various natural fiber - cement options.

Table 2.1: Summary of literature on natural fiber cement composites

Ref	Author(s)	Publication Date	Hemp Hurd	Hemp Bast	Wheat Straw	Wood Fiber	Kenaf Fiber	Sisal Fiber	Flax Fiber	Portland Cement	Lime Cement	MgO Cement	Compression	Flexural	Thermal Conductivity	Water Sorption	Impact Resistance	Other
[14]	Zhou et al.	2016		✓						✓			✓					
[15]	Stevulova et al.	2016	✓							✓			✓				✓	
[16]	Snoeck et al.	2015		✓		✓			✓	✓				✓				
[17]	de Bruijn et al.	2009	✓	✓						✓	✓		✓			✓		
[18]	Merta & Tschegg	2013		✓	✓					✓								✓
[19]	Walker et al.	2014	✓			✓				✓	✓							✓
[20]	Jarabo et al.	2012	✓							✓				✓		✓		
[21]	Awwad et al.	2012		✓						✓			✓	✓	✓			
[22]	Li et al.	2006		✓						✓			✓	✓		✓		
[23]	Ferreira et al.	2015						✓		✓		✓				✓		
[24]	Stevulova et al.	2013	✓							✓	✓		✓		✓	✓		
[25]	Diquélou et al.	2016	✓							✓	✓		✓	✓				
[26]	Merta	2016		✓						✓			✓					
[27]	Balčiūnas et al.	2015	✓							✓	✓		✓		✓			
[28]	Diquélou et al.	2015	✓							✓			✓	✓				
[29]	Awwad et al.	2014		✓						✓				✓				
[30]	Li et al.	2004		✓						✓			✓	✓				
[31]	Gourlay et al.	2017	✓							✓					✓	✓		

Table 2.1 (cont.): Summary of literature on natural fiber cement composites

Ref	Author(s)	Publication Date	Natural Fiber Types							Cement Types			Characterization Methods					
			Hemp Hurd	Hemp Bast	Wheat Straw	Wood Fiber	Kenaf Fiber	Sisal Fiber	Flax Fiber	Portland Cement	Lime Cement	MgO Cement	Compression	Flexural	Thermal Conductivity	Water Sorption	Impact Resistance	Other
[32]	Awwad et al.	2010		✓						✓			✓	✓				
[33]	Sedan et al.	2008		✓						✓				✓				
[34]	Arnaud & Gourlay	2012	✓							✓	✓		✓			✓		
[35]	Cantor et al.	2014			✓					✓			✓					
[36]	Muda et al.	2016					✓			✓							✓	
[37]	Elsaid et al.	2011					✓			✓			✓	✓				
[38]	Wei & Meyer	2015						✓		✓			✓		✓			
[39]	Wei & Meyer	2014						✓		✓			✓					
[40]	Page et al.	2017	✓						✓		✓		✓		✓	✓		

2.2 Classification of Natural Fibers

There have been a wide range of natural fiber and cement combinations studied in the literature. Natural fibers can be classified in three categories depending on their source: animal, plant (lignocellulosic) or mineral based fibers [41]. Lignocellulosic fibers can be further classified by the plant type and the origin within the plant [42].
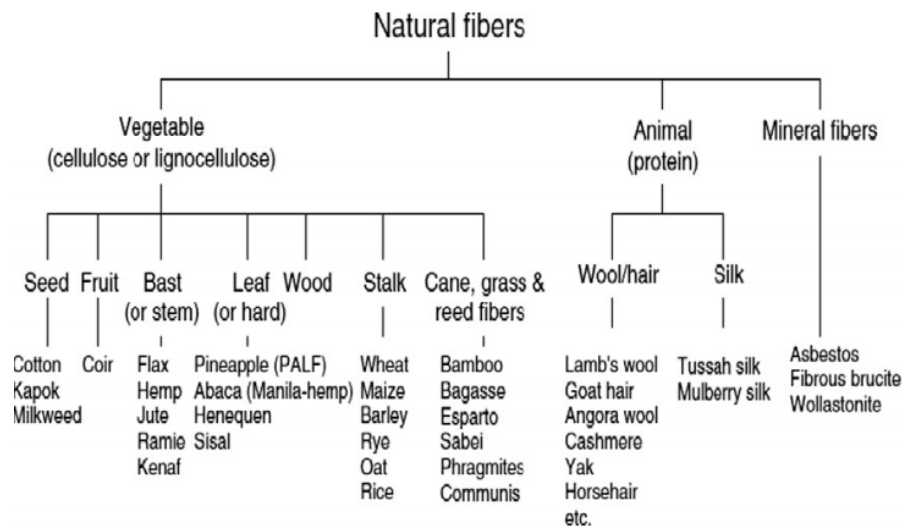
Figure 2.1: Classification of natural fibers [42].

Figure 2.1 displays a summary of the different types of natural fibers. A variety of natural fiber types have been examined in both polymer and cement based composites including hemp bast fiber [14,16-18,21,22,26,29,30,32,33], hemp hurd [15,17,19,20,24,25,27,28,31,34,40], wheat straw [18,35], flax fiber [16,40], kenaf fiber [36,37], and sisal fiber [23,38,39]. Of particular interest to Western Canadian farmers and producers are the straw components from two crop types: hemp hurd and wheat straw.

Industrial hemp (*Cannabis sativa*) can produce two types of lignocellulosic fibers: hemp bast and hemp hurd. Hemp bast fibers are harvested from the phloem (outer layers) of the industrial hemp stalk and are long and fibrous (see Figure 2.2)
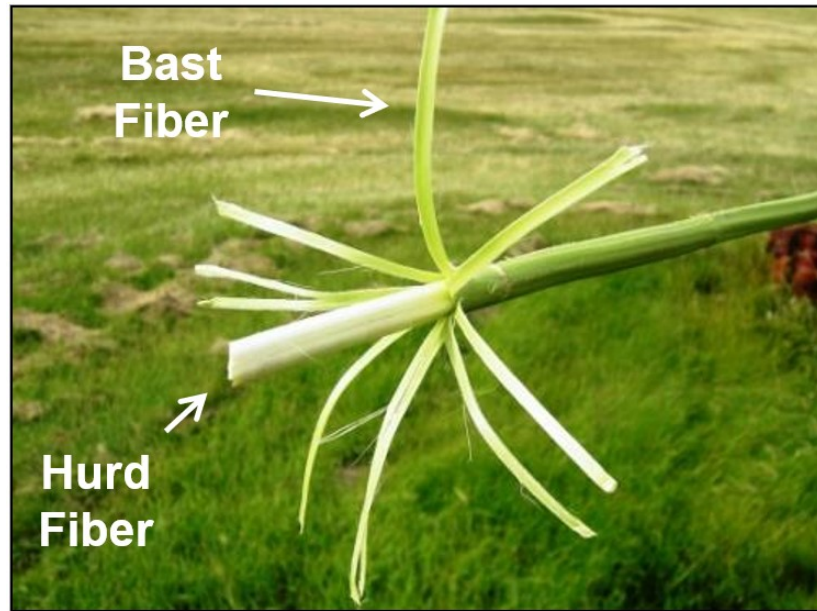
Figure 2.2: Hemp bast fiber and hurd fiber (image courtesy of Innotech Alberta)

The bast fiber's high tensile strength allows it to be used in numerous applications including textiles and composites (e.g. automotive and building products) which is why they are one of the most valuable parts of the hemp plant. As shown in Figure 2.2, hemp hurd fibers are found in the xylem of the plant (center of the stalk), and is a brittle woody material [43]. Hemp hurd (also known as shiv or shive) is a co-product of hemp processing and it's uses are somewhat limited (e.g. low cost sorbent applications for livestock bedding). Hemp hurd has a similar microstructure to that of wood, however, it has a lower density and lower mechanical properties due to its porous cell structure [44].

Another agriculture product that is common to Western Canada is wheat straw. Wheat straw also has limited non-agricultural uses, and is produced in excess during the harvesting of edible grain [6]. As shown in Table 2.2, wheat straw has lower cellulose and lignin content compared to hemp and wood which results in very low mechanical properties. In addition, wheat straw also contains a high silica content compared to wood and hemp fibers which poses other processing and compatibility issues (weaker interfacial properties, and abrasiveness during processing) [45].

Table 2.2: Chemical composition of various natural fibers as reported in the literature

Fiber Type	Cellulose (wt %)	Hemicellulose (wt %)	Pectins (wt %)	Lignins (wt %)	Ref
Hemp Bast Fiber	56.1-74.4	10.9-22.4	0.9-20.1	3.7-6	[46,47]
Hemp Hurd	44.2-44.5	27.2-32.8	-	21.03-24.4	[48,49]
Wheat Straw	24.2-39.1	22.5-24.2	-	17.5-25	[50,51]
Pine	40	28.5	-	27.7	[52]
Spruce	39.5	30.6	-	27.5	[52]

2.3 Effect of Lignocellulosic Fibers on Cement Curing Response

The interaction of natural fibers with cement during the curing process has been found to be a significant issue in a number of studies. In general, lignocellulosic particles appear to have some inhibitory effect on Portland cement hydration and curing, which results in a reduction in mechanical properties of the composite. Miller et al. [53] studied the inhibitory effect of wood fiber on cement curing, and suggested that the organic compounds in wood form chemical complexes with the metal ions present in the cement, thereby decreasing the concentration of calcium ions necessary for the cement curing reaction. The degree of inhibitory effects also was found to be wood species dependant. Sedan et al. [46] examined the inhibitory effect on cement setting times in relation to hemp fiber-matrix interaction. The authors concluded that the pectins on the surface of the hemp fibers can trap calcium from the cement. This reaction results in calcium fixation through a structure called "egg boxes" which inhibits the growth of calcium silicate hydrates therefore, delaying setting time. Conversely, Soroushian et al. [54] found that the high water and alkali solubility of wheat straw is the dominant factor affecting the physical properties of their wheat straw-cement particle boards. Additionally, the effects of pH, base buffering capacity, and acid-to-base buffering capacity ratio were also identified as significant factors affecting the inhibitory effects of extractives from natural fibers on Portland cement [55].

In addition to better understanding the mechanisms of inhibition, a number of studies have also developed strategies to counteract this inhibitory effect introduced by lignocellulosic fibers. These strategies generally fall within two categories: 1) extraction or alteration of the cement inhibitors in the fibers (e.g. sugars, tanins, pectins, hemicellulose, etc.), and 2) rapid

curing of the cement. One of the simplest treatments within the first category is cold or hot water washing of natural fibers. Miller et al. [53] reported that a substantial improvement in cement setting times can be achieved by removing water soluble extractives and sugars from wood fiber. The authors used hammer milled Larch wood particles that were boiled in distilled water for 6 hours. The results showed that the hot water extraction resulted in a decrease in cement setting times by up to 56 times compared to that of the untreated wood. Additionally, Alberto et al. [56] examined the effect of a number of fiber treatment methods on the cement setting times and temperatures (as measured by isothermal calorimetry) of cement reinforced with fibers from tropical wood species. These fibers were treated with hot water, cold water, and caustic (NaOH) solutions. Overall, the NaOH treatment displayed the highest increase in cement setting hydration temperature while the cold-water treatment displayed the lowest increase in cement setting hydration temperature. However, the relative increase between treatment option varied significantly with wood species.

In addition to the use of natural fiber treatments prior to cement mixing, rapid curing of the cement using cement additives (such as accelerators) has also been effective in mitigating cement cure inhibition by accelerating the cement curing temperature and rate [57]. Matoski et al. [58] demonstrated that cement accelerators, specifically ones containing compounds that form insoluble chelates with the organic material, displayed the highest level of inhibition reduction. Fernandez et al. [59] found that a combination of accelerators can be used to optimize the cement setting and resulting in improved mechanical properties of rice straw-cement boards. In their study, a combination of Na_2SiO_3 and $CaCl_2$ accelerators were found to increase board strength compared to the use of each accelerator separately.

2.4 Mechanical Properties of Natural Fiber – Cement Composites

The mechanical properties of natural fiber-cement composites have been investigated for a wide range of fiber types including wood [15, 20], hemp [14-22,24-34,40], wheat straw [18,35], kenaf [36,37] and sisal [38,39], and cement types including Portland cement [14-39], lime cement [17,19,25,27,34,40], and magnesium oxide cements [24]. In addition, many of these studies have also examined composite material design aspects (such as fiber fraction) and fiber processing effects (such as fiber size distribution).

In general, the addition of natural fibers to cement has been found to reduce both compression strength [59-61] and compression modulus [59,60], especially at higher weight fractions. Li et al. [22] studied the effect of fiber fraction on the compressive strength of natural fiber-cement composites. The authors suggest that there is a negative linear relationship between the fiber content and the compressive strength of hemp fiber- cement composites: as fiber volume fraction increases compressive strength tends to decrease. Additionally, as fiber size increases, the compression strength decreases. The authors proposed that the observed reduction in compressive strength is due to an increase in porosity of the composite due to the addition of fiber. This phenomenon is also demonstrated by Murphy et al. [60] in a study that investigates the physical properties of lime-hemp concrete. As the fiber content in the hydrated lime mixes and the hydraulic and pozzolanic mixes increases the compressive strength of the composite decreases. Again, the author attributes the compression strength difference to the compaction and density of the composite. This behavior is also seen in wheat straw cement composites. Farooqila et al. [61] demonstrated that the addition of natural wheat straw and

treated wheat straw into a concrete mixture at 3% by mass of cement reduces the compression strength of the concrete by 10% and 26% respectively. The authors treated wheat fibers by boiling them for 2 hours to increase interfacial chemical and mechanical bonding. This treatment had a contrasting effect on the elastic modulus of the composite where it was shown to decrease it by 32%. Bruijn et al. [17] studied the effects of using different cements with a combination of hemp hurd (shives) and bast fibers on several properties of the composite. Five mixes were used in this study with varying proportions of hydrated lime, hydraulic lime and Portland cement. Additionally, a mixture of hemp fiber and hemp hurd (shive) was used at 30% of the weight of the cement (weight fraction). The authors concluded that a mixture of fiber types did not have a significant effect on the mechanical properties of the composites, however, the composites made using Portland cement had a higher compressive strength and elastic modulus compared to the unreinforced cements. These results support the assumption that the mechanical properties of the composite are largely governed by the mechanical properties of the cement.

In terms of flexural (bending) properties, the addition of natural fibers to cement has been generally found to increase flexural strength [16, 46, 60]. The influence of the addition of hemp fiber on the flexural strength of the cement composites has been investigated by Sedan et al. [46]. It was found that the addition of 16 vol% of hemp bast fibers increased the flexural strength of the composite by 40% and decreased the elastic modulus by 25% relative to unreinforced cement. The authors also tested flexural samples with hemp fibers enhanced with an alkali pre-treatment. The resulting specimens saw a further increase in flexural strength by 94% relative to the unreinforced cement most likely due to enhanced bonding between the fiber matrix interface. Murphy et al. [22] demonstrated a high correlation between flexural strength and

binder properties at low fiber content. Additionally, a maximum flexural strength was attained at 50% hemp content due to the lime-hemp bonds. Li et al. [22] has displayed that increasing hemp fiber content increases flexural strength linearly up to a fiber aspect ratio of 150. The authors demonstrated that flexural strength and flexural toughness are correlated with fiber content. Since cracks in the matrix are unable to extend without debonding the fibers, it requires more energy to fracture the composites in the presence of hemp fibers.

2.5 Thermal Insulation Properties of Natural Fiber – Cement Composites

The thermal insulation properties of natural fiber-cement composites has also been investigated for a wide range of fiber types including hemp [21,24,27,31,40], flax [40], and sisal [38], and cement types including Portland cement [21,24,27,31,38], lime cement [24,27,40], and MgO cement [24]. A number of these studies have also investigated effect of fiber particle size [24], composite density [65,66], and fiber particle size on thermal properties.

Stevulova et al. [24] investigated the effects of hemp particle length on the thermal conductivity of hemp hurd, MgO cement composites. It was observed that lower thermal conductivities (more insulative) were measured for composites with larger particle sizes. The authors postulated that the hemp particles effectively act insulating voids, thus reducing thermal conductivity in the cement. The larger the particle size, the greater the insulating effect.

Sinka et al. [62] studied the effects of several alternative cementitious binders on the thermal insulation properties of hemp hurd reinforced composites. It was found that the thermal conductivity of their composites had a direct correlation with density which has was also been

shown by Balčiūnas et al. [63]. The authors suggest that this correlation is due to the increase in contact zones in the denser mixtures. This in turn leads to a larger thermal conductivity and translates to a lower R-value. Awwad et al. [21] examined the use of hemp bast fiber as a method for reducing coarse aggregates in concrete. It was found that the addition of 0.75-1 vol% hemp fiber to concrete results in a decrease in thermal conductivity by 25-35%. It was suggested that the reduction in overall thermal conductivity was due to the low thermal conductivity of the hemp fibers thus reducing the heat flux through the multiphase material.

2.5 Water Sorption Behavior of Natural Fiber – Cement Composites

Lignocellulosic fibers are known to possess hydrophilic properties (affinity to water uptake) due to the presence of cellulose and hemicellulose molecular structures [48,49]. As a result, there has been a number of studies examining the moisture sorption behaviour of natural fiber-cement composites.

Stevulova et al. [48,49] studied the water sorption behavior in hemp hurd cement composites made with Portland and MgO cements [48,49]. The authors observed that, in the short term, the mean particle length had a significant effect on water sorption: as the mean particle length increased the water sorption of the sample increased. Conversely, Bruijn et al. [17] performed studies on similar materials but found no significant differences in water sorption coefficients, suggesting that moisture sorption is not affected by cement type.

While the moisture sorption behavior in natural fiber composites has been studied experimentally, there has been relatively little modelling effort for these materials. This is in stark contrast to the breadth of moisture sorption models that have been proposed and developed for

synthetic fiber composites (e.g. glass and carbon fiber polymer composites). Shen et al. [64]

presented a method for determining the moisture content in synthetic composites as a function

of time. The authors were interested in determining the effects of moisture content relative to

mechanical properties of composite materials. Their approximation was based on a thin plate

exposed on two sides to a wet environment, and assumed a one-dimensional problem where the

moisture varied within the thickness of the sample. The authors used Fick's law as a basis for the

approximation which assumes that diffusion is based on the molecular movement of water

particles through a material.

Mbou et al. [65] employed a similar approach when investigating the water absorption

kinetics of the pith of wine palm (Ra*phi*a *v*inifera). In this study, the experimental data was

compared to eleven theoretical models to determine the best fit model. It was determined that

the water absorption behaviour for the *Raphia vinifera* plant followed Fick's second law model

with two-stage absorption. Additionally, the authors suggest that the diffusivity differs within the

pith depending on the sampling position and distance from the center of the pith (with the center

displaying the highest initial diffusivity).

3.0 Materials and Methods

3.1 Materials

Two natural fiber types were assessed in this study: 1) hemp hurd and 2) wheat straw. The hemp hurd (hammer mill decortication system) was provided by InnoTech Alberta (Vegreville, Alberta). The wheat straw was obtained in a 680 kg bale from Fabiyan Ranch (Wainwright, Alberta). For the wheat straw, the outer portion of the bale was discarded due to potential contamination and damage, and only dry straw from the middle of the bale was used. The straw was then separated from the bale and laid out to dry indoors at 20°C for 3 days prior to further processing. Once dry, the wheat straw was then processed using a hammer mill (Bühler/ Farm King) with a 7.6 mm circular opening sieve.

The cement used in this study was a general use Portland cement (Type 10, Quikcrete), and was selected due to its use in concrete and other applications. This cement also complies with ASTM C 150, and has a working time of 60 minutes. A non-chloride accelerator (Fritz-Pak) was also utilized in this study to aid in the cement curing process and improve the final properties of the samples. The accelerator was added according to the manufacturer's instructions (2% by weight of cement used).

3.2 Composite Specimen Manufacturing

3.2.1 Material Sizing and Characterization

For both hemp hurd and wheat straw, the fibers were sieved into various fiber size groups using a sieve shaker (Gilson Global Test Master). This sieve shaker contained 7 mesh trays of varying opening sizes (12.5 mm, 6.3 mm, 5 mm, 3.15 mm, 2.5 mm, 1.25 mm, and 0.6 mm) and a dust collection pan at the bottom. Bulk fibers were slowly added to the top of the unit, and through agitation, fell through the series of sieves (each with a decreasing opening size as the fibers progressed towards the bottom). From these sieves, different fiber sizes were collected and grouped into three categories: a) a "coarse" fiber group, b) a "fine" fiber group, and c) a rejected group (not used in the study). For the "coarse" fiber category, fibers from the 3.15 mm and 2.5 mm trays were combined (in equal amounts from each tray), while for the "fine" category, fibers from the 0.6 mm tray were used. These fiber groupings were then used as inputs in the manufacturing of the cement composites.

In addition to fiber separation and sizing, the density of both the fibers and cement was also determined. Simple bulk density measurements (measured mass divided by the volume) were taken for the cured cement (after a cure time of 28 days) which was used to determine the volume fraction of constituents in the final composite. The density of both types of fibers was measured using a pycnometer (AccuPyc II 1340 Series) with nitrogen gas displacement. This latter method was chosen for the fibers since pycnometry measurements represents the average densities of individual fiber particles embedded in the cement. Bulk density measurements of fibers include spaces and gaps between fibers which are not present in the

actual composite samples. In both cases, each density measurement was repeated 3 times to quantify variability of the results.

3.2.2 Fiber-Cement Mixing

The fiber-cement mixing procedure is a critical step in the specimen manufacturing process. This procedure was designed to attain repeatable results, and to maximize the homogeneity of the composite samples in order to minimizing errors. An overview of the fiber-cement mixing procedure is shown in the flow chart in Figure 3.1.
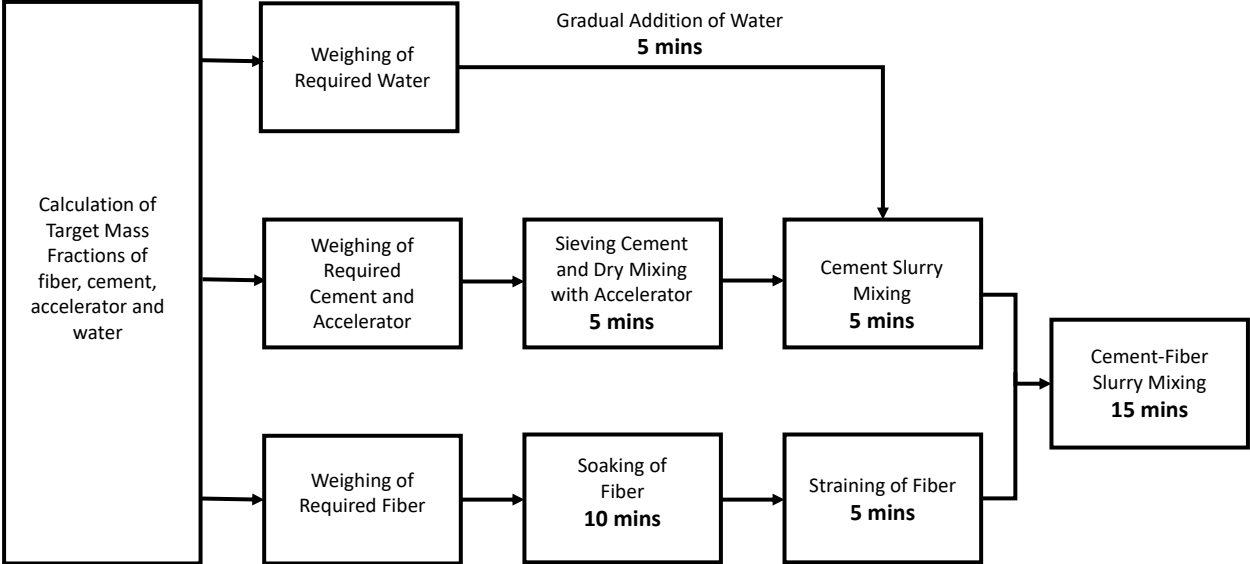
Figure 3.1 Overview of fiber-cement mixing procedure

3.2.2.1 Composite Mix Design

In the first step, mix ratios of fiber, cement, water and accelerator were calculated based on the targeted fiber volume fractions of the final composite, and recommended water-cement and cement-accelerator ratios. The mix design was based on four target fiber volume fractions in the final composite specimens: 0% (control; unreinforced cement), 5%, 10% and 15%. The use of volume fraction to characterize composite mixtures (as opposed to weight fraction) allows accurate comparison between fiber types with varying densities, and also represents a key parameter in modelling the behaviour of composite materials [66].

The mass ratio of matrix (cement) to fiber for a given target volume fraction of fiber in the final composite was determined based on the following equations. The volume fraction of fiber is determined by the following equations:

$$V_C = V_f + V_m \tag{1}$$

$$v_f = \frac{V_f}{V_c} = \frac{V_f}{(V_f + V_m)} \tag{2}$$

where V_f is the volume of fibers (in m³), V_m is the volume of matrix (in m³), V_c is the volume of composite (in m³), v_f is the volume fraction of fibers (non-dimensional), v_m is the volume fraction of the matrix (non-dimensional), and v_c is the volume fraction of fibers (non-dimensional).

By rearranging equation 2, the volume of matrix (cement) can be calculated as follows:

$$V_m = \frac{V_f}{v_f} - V_f \tag{3}$$

Next, the volumes of the constituents can be calculated from their masses and densities by using the following equations:

$$V_f = \frac{M_f}{\rho_f} \qquad (4)$$

$$V_m = \frac{M_m}{\rho_m} \qquad (5)$$

where M_f is the mass of fibers (in g), M_m is the mass of matrix (in g), ρ_f is the density of the fibers (in g/m^3), and ρ_m is the density of the matrix (in g/m^3).

Inserting equations 4 and 5 into equation 3 (and with some rearrangement), the mass ratio of matrix to fiber required to achieve a target volume fraction of fiber in the final composite mix can be calculated, as shown in Equation 6.

$$\frac{M_m}{M_f} = \frac{\rho_m}{\rho_f}\left(\frac{1}{v_f} - 1\right) \qquad (6)$$

Equation 6 was used in determining the mass ratios of the matrix (cement) and fiber for the various targeted final fiber volume fractions of the composites tested (i.e. 0%, 5%, 10% and 15% volume for fiber to cement).

In order to ensure proper curing of the cement matrix, a water-cement ratio (M_w/M_m) of 0.4 by mass was selected based on guidance from the literature in order to properly complete the cement hydration reaction [67]. Since lignocellulosic based natural fibres are known to

absorb water, all fibers were pre-soaked to saturation prior to mixing with the cement slurry in order to maintain this water-cement ratio. If this pre-soaking is not performed, the natural fibers will take water from the wet cement mixture which may result in diminished cement matrix properties. Note that the density of the cement matrix in Equation 6 is the measured bulk density of the cured cement at 0.4 water to cement ratio (after curing for 28 days) as this accounts for volume change due to the curing process and water evaporation.

A dry cement accelerator (Fritz Pak NCA) was also added to the dry cement at a ratio of 0.02 g accelerator per 1 g of cement based on the manufacturer's recommendation. The addition of a cure accelerator counteracts possible inhibitory effects introduced by lignocellulosic fibers, as discussed in Section 2.3. This was done prior to cement-fiber mixing (see sections below).

3.2.2.2 Fiber Washing and Saturation

For the mixing steps, dry fiber was first weighed out according to the fiber mass fraction derived from the target fiber volume fraction of the mix. The fiber was then placed in a large plastic bag which is subsequently filled with potable water to saturate all the particles. The fiber was left in water for 10 minutes with frequent agitation to facilitate the water absorption process. Holes were then poked at the bottom of the plastic bag to allow the excess water to strain out for 5 minutes.

This process is crucial as it not only saturates the fibers with water thus minimizing water absorption from the cement slurry and maintaining a constant water-cement ratio but also it washes away dust and other compounds from the surface of the particles, enhancing the fiber-cement bond. Additionally, in the case of the wheat straw, this washing technique separates out

residual wheat grains that may remain with the fiber particles after processing and sizing. Wheat grains are composed of 60-75% starch, a polymer of glucose, which is known to drastically decrease the compression strength of cement [68]. A photograph of residual wheat grains collected after washing is shown in Figure 3.2.

Figure 3.2 Wheat grain separated from wheat straw by the process of sedimentation.

For each fiber type and size, the percent water absorbed (by mass), m_{wa}, during the saturation procedure was calculated using Equation 7.

$$m_{wa} = \left[\frac{M_{fsat} - M_{fi}}{M_{fi}} \right] x\ 100 \qquad (7)$$

where M_{fsat} is the mass of fibers after saturation (in g), and M_{fi} is the mass of the dry fibers prior to saturation (in g).

3.2.2.3 Mixing Procedure

Pre-weighed cement (based on the selected fiber mass and Equation 6) was gradually sieved through a 1 cm metal mesh to remove any clumping or compaction that may have occurred due to the storing and stacking of the cement bags. Any residual clumps were further broken down by hand, and re-sieved until a uniform dry cement powder was obtained. The cement was then placed in a 170 liter portable cement mixer (YARDMAX) along with the pre-measured accelerator powder, and a plastic cover was placed on the opening of the mixer to reduce the dust released during mixing. The cement mixer was then turned on and the dry cement/accelerator mixture was homogenized for 5 minutes to achieve an even distribution of the accelerator throughout the cement.

After the homogenization of the cement-accelerator mixture, the plastic cover was removed, and the wet mixing process was started. The mixer was turned on and a pre-weighed amount of water (based on Equation 6) was gradually added to the dry mix in 250 ml increments. This gradual addition of water to the cement was done over 5 minutes, and was further mixed for an additional 5 minutes to achieve a smooth and homogenous slurry. This procedure was found to prevent the cement from forming spherical clumps, and facilitated uniform hydration. Once the cement and water were mixed, presoaked fibers were added to the slurry and mixed for 15 more minutes until all the particles were uniformly coated.

3.2.3 Specimen Molding and Curing

After the wet fiber-cement mixture was prepared, the next step was specimen molding and curing. An overview of these steps is shown in the flow chart in Figure 3.3.

```
┌──────────────┐        ┌──────────────┐        ┌──────────────┐        ┌──────────────┐
│ Cement-Fiber │        │  Samples are │        │  Samples are │        │  Samples are │
│ Slurry Poured│ 2 Days │  Demolded and│ 7 Days │ Removed from │19 Days │  Prepared and│
│ into Molds and│──────▶│ Submerged into│──────▶│Water and Left on│────▶│ Mechanical Tests│
│  left to set │        │     water    │        │ Curing Racks │        │   Performed  │
└──────────────┘        └──────────────┘        └──────────────┘        └──────────────┘

        ┌────────────────────────────────────────────────────────────┐
        │            Total of 28 Days of Curing                       ───▶
        └────────────────────────────────────────────────────────────┘
```
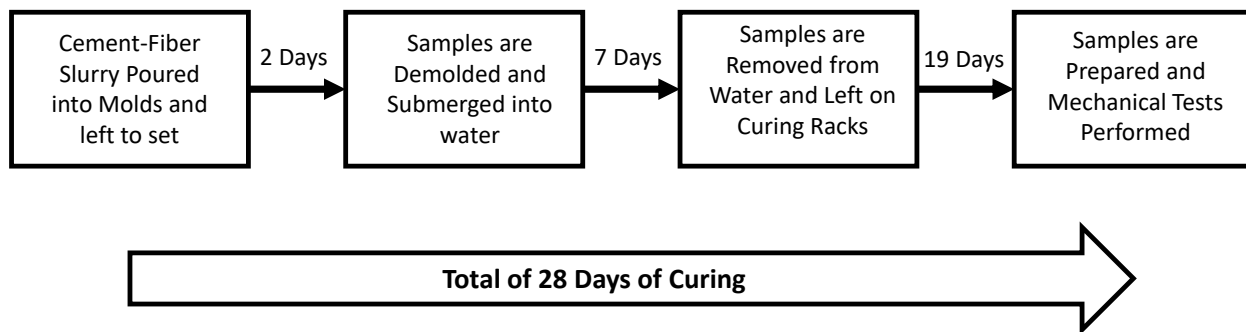
Figure 3.3 Sample molding and curing procedure

Three types of molds were used in this study, as shown in Figure 3.4. For compression tests, a standard cylindrical mold (HM153, Gilson Global) with dimensions of 76 mm in diameter and 152 mm in length was used. For flexural tests, a rectangular beam type mold (HM-288, Gilson Global) with dimensions 101 mm in height, 101 mm in depth and 380 mm in length was used. Both the cylindrical and beam molds were plastic moulds that were compliant with various standards (ASTM C192/192M, ASTM C31/31M, ASTM C470/470M, ASTM C293/293M, and ASTM C78/78M). rectangular beam molds were used model number.

For the insulation tests, there was no standard mold that could be obtained. As such, a custom-built mold was fabricated. The molds were designed to produce a 304 mm x 304 mm x 25 mm flat panel which can fit in the guarded hot plate apparatus. The molds were fabricated

using plywood (19 mm thickness), and were then sealed internally using a smooth 304 mm x 304 mm Kydex plastic sheet inner shell (3 mm thickness) to allow for easy demolding. The plastic was cut to size and the edges were secured using M3 masking tape. Figure 2.2 presents the molds used to manufacture the thermal insulation, compression, and flexural samples. The flexural and thermal insulation molds were cleaned thoroughly between each mix and reused (reassembled in the case of the thermal insulation molds) while the compression molds were only used one time due to deformation to the molds during the demolding process.

a)   b)   c)
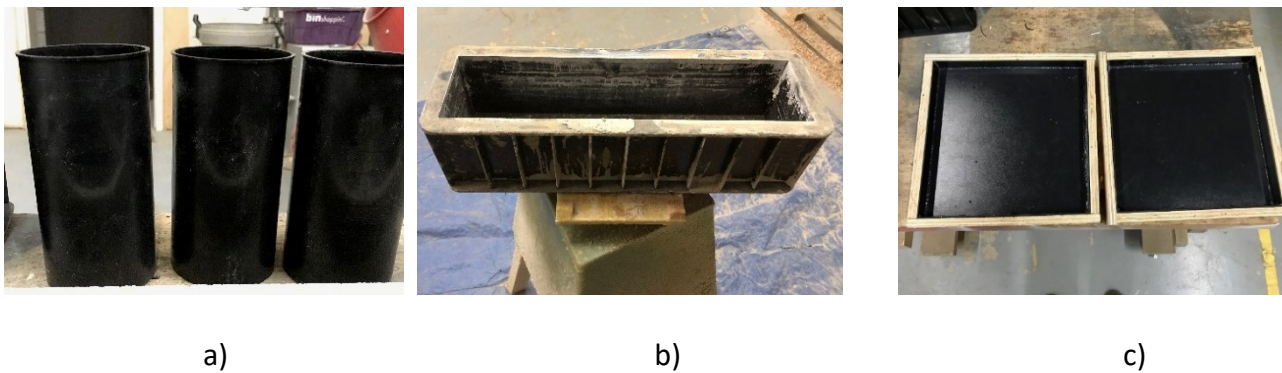
Figure 3.4 Specimen molds used for a) compression testing b) flexural testing, and c) thermal insulation testing

The mixture was poured into the molds to a specified height, and tamped 20 times by lightly tapping the bottom of the molds against a table to facilitate compaction and reduction of voids. The slurry was homogenized in between pouring of the individual molds by turning on the mixer for 4 full revolutions of the drum. This was done to obtain a representative sample in each specimen by reducing any settling effects in the mixer.

The filled molds were then covered with a plastic film which reduced water evaporation and maintain the required water-cement ratio to complete the hydration process. These covered molds were then left to cure for 2 days in indoor laboratory conditions (19.57°C average temperature of and 41.76% relative humidity). After this initial curing period, the hardened samples from each mix were demolded and placed in a water bath for 7 days to ensure complete curing of the cement matrix. The samples were then removed from the water bath and placed on a drying rack in ambient conditions (air dry) for an additional 19 days to continue the final curing process. Overall, the cure cycle took 28 days from start to finish, at which point the specimens were ready for final specimen preparation prior to testing.

3.2.4 Final Specimen Preparation

Prior to testing, all samples were surfaced to eliminate irregularities associated with open mold surfaces, and final measurements of all dimensions and mass were taken. The ends of the cylindrical compression samples were cut (perpendicular to the cylinder axis) using a cut-off saw (Dewalt) to attain a flat and perpendicular surface suitable for compression testing. Conversely, the flat faces of the thermal insulation plates were sanded to remove the as-molded top layer and the sedimented cement bottom layer to expose the internal structure of the plates to the thermal insulation sensors. Additionally, the thermal insulation samples were sanded in pairs since the guarded hot plate apparatus requires two specimens of equivalent thicknesses per test. The thermal insulation plates were gradually sanded using an industrial Bell Saw plywood sander at 1 mm increments to avoid damaging the samples.

In terms of the moisture absorption samples, two specimens were cut from the thermal insulation panels after completion of the thermal insulation tests (i.e. thermal test were non-destructive in nature, and specimens were re-used for moisture sorption characterization). To fabricate the moisture sorption specimens, two thermal insulation panels were chosen from the 6 plates fabricated for each test condition (fibre type, fiber volume fraction and fiber size). Using these two panels, two 101 mm x 101 mm water absorption test samples were cut from each panel for a total of 4 replicates per test. These samples were cut using an MK diamond wet tile saw and a segmented blade. Since these water absorption specimens were cut using a wet saw, they were subsequently oven dried for 4 days at 82℃ to ensure a starting moisture content of 0%. The weight of the samples was recorded every 24 hours to ensure a plateauing equilibrium. Afterwards, the samples that were yet to be tested were stored in sealed plastic bags to maintain the original moisture content of 0%.

After all the test specimens were cut and/or sanded, their final dimensions were measured, and each sample was weighed. The dimensions taken for each cylindrical sample included the mean diameter (taken as the average of eight measurements at 45° increments around the circumference at both the top and bottom of the cylinder), and the mean height (taken as the average of four measurements at 90° increments around the circumference). For the flexural test specimens, the mean dimensions were determined by measuring width and depths of the beams (two measurements each) using calipers at 4 equally spaced points along their length, and by measuring the length of the sample at each of the 4 sides. For the thermal insulation plates and the moisture absorption samples, 4 thickness measurements were performed along each side of the samples (at the mid-point).

Once final preparation and measurements of the specimens were completed, they were then ready for testing. All mechanical tests (compression and flexural) were performed on prepared samples immediately after the 28 day cure cycle.

3.2.5 Final Test Matrix

In total, the test matrix used in this study consists of 13 unique mixes based on 2 fiber types (hemp hurd and wheat straw), 3 fiber fractions (5%, 10%, 15%), 2 fiber size ranges (coarse and fine), and 1 unreinforced cement control (i.e. [2 x 3 x 2] + 1 = 13). In terms of nomenclature, the following specimen designation was used throughout the document to identify each unique sample based on the three variables being investigated: fiber type, fiber size, and fiber volume fraction, as shown in Figure 3.5.

XX-Y-ZZ

Fiber Volume Fraction (in %):
0 (control)**, 5, 10, 15**

HH – Hemp Hurd
WS – Wheat Straw

C – Coarse Particle Size Range
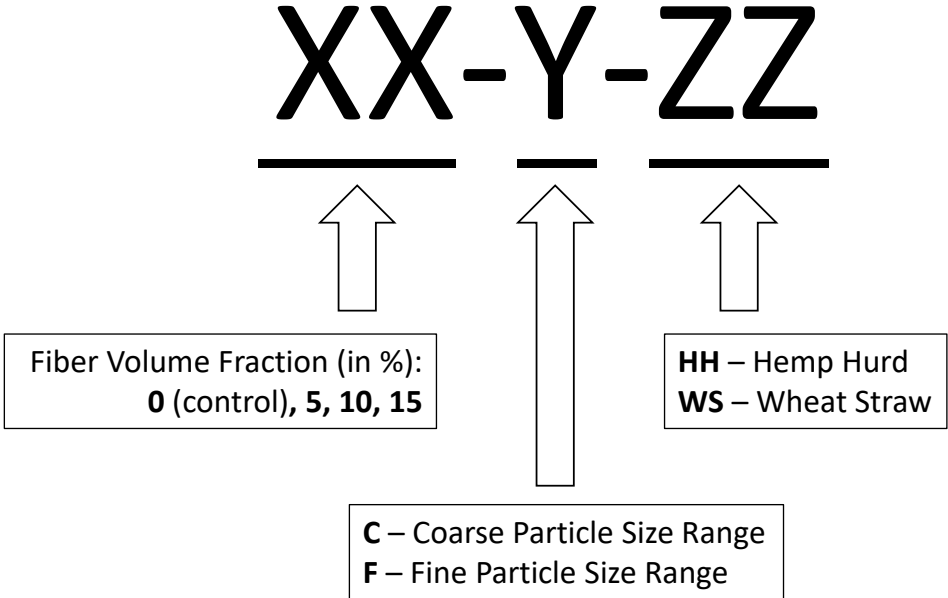**F** – Fine Particle Size Range

Figure 3.5 Test specimen nomenclature for various paramaters considered (fiber volume fraction, fiber size and fiber type)

3.3 Specimen Testing

3.3.1 Mechanical Testing

3.3.1.1 Compression Testing Methodology

Compression tests were performed using ASTM standard C39/C39M-17b (Standard Test Method for Compressive Strength of Cylindrical Concrete Specimens) as a guideline. This standard was chosen as it describes a procedure for testing the compressive strength of a cylindrical concrete specimens with a density higher than 800 kg/m^3. All mechanical tests were performed at TTS Services (Edmonton, AB), with compression tests being performed on one of two testing machines due to limitations of the load cell ranges. For test capacities up to 7,000 kgf, a modified Instron (TTS UTM-2) universal testing machine was used, while for test capacities greater than 7,000 kgf, a modified Instron (TTS-FSTM-1) universal testing machine was utilized (maximum load of 22,671 kgf). Both of these universal testing machines were equipped with certified and calibrated load cells (Transducer Technologies). All 10% and 15% fiber volume fraction samples were tested on the UTM-2 while the controls and 5% fiber volume fraction samples were tested on the FSTM-1. A photograph of the compression test setup is shown in Figure 3.6.

For testing, the samples were initially placed in the load frame, and were preloaded to 20 kgf at which point the load cell was zeroed. Compression tests were conducted under displacement control at a rate of 1 mm/min. During the test, the compressive load (kgf) values were recorded every 10 seconds using a PC computer connected to the load cell. Tests were continued until specimen failure occurred denoted by a noticeable drop measured force and/or

observed fracture of the specimen. The compressive failure strength (in MPa) was calculated by dividing the maximum load (converted to N) by the cross-sectional area of the specimen tested (based on average diameter measurements). In total, 4 replicates were tested per unique test condition.


Figure 3.6 Photograph of compression test setup

3.3.1.2 Flexural Testing Methodology

Four-point flexural (bend) tests were performed using ASTM standard C78/C78M-18 (Standard Test Method for Flexural Strength of Concrete) as a guideline. The test was performed on a modified Instron universal testing machine (TTS-UTM-1) with flexural supports with span

lengths of 300 mm for the lower support and 100 mm for the upper support. A schematic and photograph of the flexural test setup is shown in Figure 3.7.

For testing, the samples were initially placed in the loading frame (with the smooth, as-molded sides at top and bottom), and were preloaded to 3 kgf at which point the load cell was zeroed. Flexural tests were conducted under displacement control at a rate of 1 mm/min. During the test, the load (kgf) values were recorded every 10 seconds using a PC computer connected to the load cell. Tests were continued until specimen failure occurred denoted by a noticeable drop measured force and/or observed fracture of the specimen. The flexural failure strength was calculated using the equation in the standard based on the maximum load (converted to N) and the average geometrical properties of the test specimen (in mm). In total, 3 replicates were tested for each test condition.
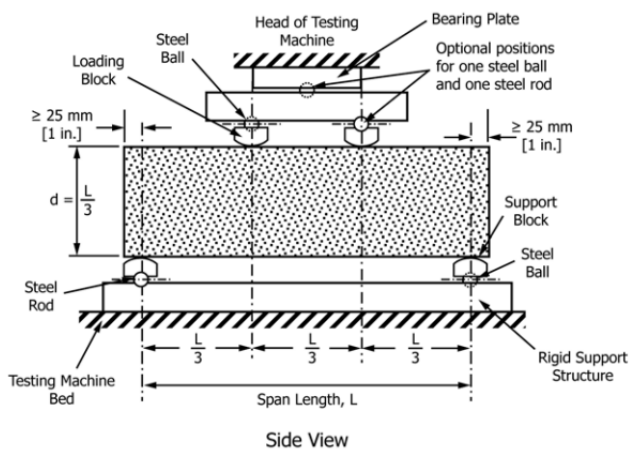
a)   b)

Figure 3.7 Flexural testing setup for four-point bending: a) schematic of standard test setup [1]according to ASTM C78/C78M-18[1], and b) photograph of current experimental setup.

---

[1] Figure reproduced with permission

3.3.2 Thermal Insulative Testing

Thermal insulation tests were performed using ASTM standard C177-19 (Standard Test Method for Steady-State Heat Flux Measurements and Thermal Transmission Properties by Means of the Guarded-Hot-Plate Apparatus) as a guideline. A DRH-300 Heat Conduction Modulus Testing Instrument was used to determine the thermal conductivity per inch of material (R-value/inch). The experimental setup is similar to the Guarded hot plate set up illustrated in ASTM C177-19 however, it is vertically oriented. Figure 3.8 shows the experimental set up relative to the arrangement illustrated in the ASTM C177-19 standard. The composite plate specimens used in these tests were conditioned in ambient lab environment 19.57°C average temperature of and 41.76% relative humidity) for an average of 3 months prior to testing.

For each test run, two composite plates of equivalent thickness were required. In total, 3 replicates per test condition was tested (i.e. a total of 6 thermal insulation plates were manufactured to achieve 3 replicates). The guarded plate test setup is composed of two isothermal cold plates that are cooled using a coolant circulating system set to maintain the two cold plate temperatures at 16°C and the one guarded hot plate temperature at 36°C. The guarded hot plate is compromised of a 225 cm² metered section in the center that is surrounded by a thermally isolated guard. The test specimens were inserted on either side of the hot plate, and were fastened in place to maintain contact with each of the cold plates on either side. The hot plate (in the middle) produces a heat flow per unit time through the test volume (measured in watts). The heat guard is designed to reduce the amount of vertical heat flow, therefore 'guarding' the heat and isolating the heat flow through the central metered section.
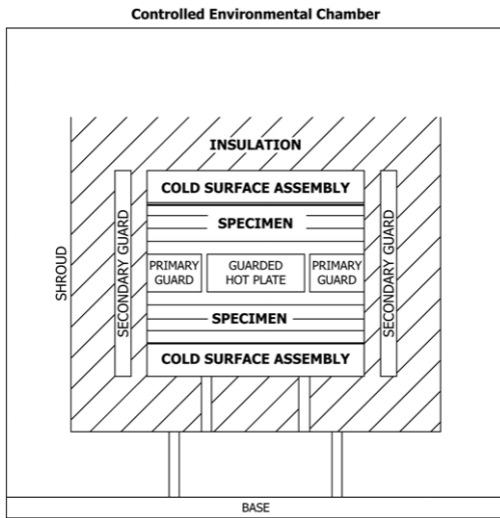
a)   b)

Figure 3.8 Guarded hot plate setup a) General arrangement of mechanical components of the guarded-hot-plate apparatus according to ASTM C177-19 [2] and b) The DRH-300 Heat Conduction Modulus Testing Instrument used in this study

When a test is started, the system begins by establishing a thermal steady state that is defined as the state where the temperature of the hot and cold surfaces are stable (i.e. heat transfer through the metering area is steady state). These conditions were maintained for at least 2 hours, prior to taking final measurements. Once the thermal steady state was achieved, 5 data acquisition runs were performed. The system outputs the measured surface temperatures T [°C], the energy output Q [W], average sample thickness d [m], sample resistance R [m²k/W], and thermal conductivity λ [W/mK]. Equations (13-14) were then used to determine the thermal resistance of the samples (also known as the "R-Value"):

$$\lambda = \frac{Qd}{2A \cdot \Delta T} \tag{8}$$

---

[2] Figure reproduced with permission

$$R = \frac{d}{\lambda} \tag{9}$$

where A is the area of the metered section of the hot plate and is equal to 0.045 m^2, and ΔT is the temperature difference between the cold and the hot side (in degrees Kelvin).

After the guarded hot plate test were completed, the moisture content of each thermal insulation panel was determined gravimetrically by placing them in a convection oven at 110°C, and then measuring mass loss at regular intervals until it reached equilibrium (fully dried or 0% moisture content). The moisture content of the insulative samples (m_{ins}) was calculated as the % change in mass before and after drying as per Equation 9, as follows:

$$m_{ins} = \left[\frac{M_{bd} - M_{ad}}{M_{bd}} \right] x\ 100 \tag{10}$$

where M_{bd} is the mass of composite plates before drying (in g), and M_{ad} is the mass of the composite plates after drying (in g).

3.3.3 Water Sorption Testing

Water sorption tests were performed on composite samples to better understand how these materials behave when exposed to ambient (outdoor) moisture conditions. Tests were performed by immersing composite samples in water, and monitoring the mass increase (water uptake) over time. As detailed in Section 3.2.4, immersion test specimens were prepared from the insulation test panels (once those tests were completed), and were completely dried prior to sorption testing. For testing, the samples were immersed in a water bath at ambient temperature

(approximately 21°C), and the mass change was recorded at regular intervals up to 48 hours. At each interval, the samples were removed and placed on a drying rack for 2 minutes to drain the excess water. Then the samples were weighed, and subsequently returned to the water bath for further exposure. The moisture content, m_{water} (in %) was determined based on changes in mass over time as per Equation 11, as follows:

$$m_{water} = \left[\frac{M_t - M_0}{M_0}\right] x \ 100 \tag{11}$$

where M_t is the measured mass of the immersion specimen at time t (in g), and M_0 is the initial mass of the fully dried immersion specimen (in g). In total, 4 replicates were tested for each material combination.

3.3.4 Experimental Statistical Methods

A statistical analysis was performed on the compression, flexural, and thermal tests to determine statistical significance. The analysis was performed using IBM SPSS statistical software. A Levene's Test of Equality of Error Variances was performed on each dataset to confirm the homogeneity of variance assumption as part of an ANOVA test with a 95% confidence interval. Additionally, a Post Hoc test was performed to determine significantly different groups.

3.4 Modelling of Water Sorption

Using the experimental sorption curves (as outlined in section 3.3.3), the diffusivity and moisture sorption profiles were predicted using a model presented by Shen et al. [64]. This model was originally developed to predict the moisture sorption mechanics of synthetic fiber reinforced composite plates. For this model, the following assumption are made:

- The model assumes sorption in a thin plate (see Figure 3.9). The thin plate has a ratio of sample thickness to length or width being much less than 1 (i.e. n/L<< 1 and n/W << 1). As such, the model assumes that water penetrates the specimens only through faces W-L, and ignores moisture sorption at the edges (i.e. through the n-L and n-W faces).

- The samples are exposed to water on both surfaces with both sides being parallel.

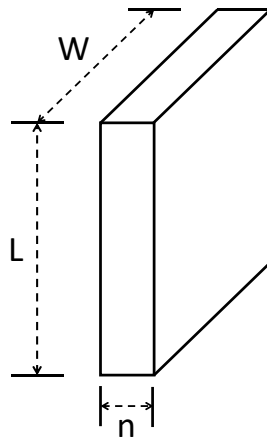- The temperature and moisture distribution within the material are initially equal.

Figure 3.9: Moisture absorption sample geometry where L is sample length (mm) W is sample width (mm) and n is sample thickness (mm)

The model is derived based on Fick's second law of mass transfer through solids [64]. Considering an infinite plate as shown in Figure 3.9 where the moisture content varies only in the x direction, Fick's law states:

$$\frac{dc}{dt} = \frac{d}{dx} D_x \frac{dc}{dx^2} \tag{12}$$

With the following initial and boundary conditions:

$$c = ci \qquad\qquad 0 < x < n \qquad\qquad t = 0$$

$$c = ca \qquad\qquad x = 0 : x = n \qquad\qquad t > 0$$

where ci is the initial moisture content is constant inside the plate and ca is the constant moisture content of the moist environment. D_x is the mass diffusivity of the material, and is a measure of water sorption rate in the x direction. Since D_x is constant and does not change with increasing moisture content, equation (12) can be simplified to [67,68]:

$$\frac{dc}{dt} = D_x \frac{d^2c}{dx^2} \tag{13}$$

Equation 13 can be solved with the above initial and boundary conditions and integrated over the thickness of the sample. The result of this integration provides a time dependent variable G:

$$G = \frac{m_t - m_i}{m_\infty - m_i} \tag{14}$$

where m_t is the weight of the moisture in the material at a time t, m_i is the initial weight of the moisture in the material prior to the exposure to a moist environment, and m_∞ is the weight of the moisture in the material when it is full saturated.

Equation 15 provides an analytical approximation for G:

$$G = 1 - ex\,p\left[-7.3\left(\frac{Dt}{n^2}\right)^{0.75}\right]$$

(15)

where t is time [min], D is the diffusivity [mm^2/min], and n is the thickness of the specimen [mm].

The moisture content of the material, M_t, at any time t is approximated as:

$$M_t = G(M_\infty - M_i) + M_i$$

(16)

where M_∞ is the saturation moisture content, and M_i is the initial moisture content. However, since the samples are oven dried prior to the test, Equation 16 can be expressed as follows:

$$M_t = M_\infty\left(1 - ex\,p\left[-7.3\left(\frac{Dt}{n^2}\right)^{0.75}\right]\right)$$

(17)

The experimental diffusivity of the specimen is calculated by plotting the experimental moisture content versus $\sqrt{t}$. This yields a curve with a linear initial portion. The diffusivity is then calculated by allocating two points on this linear portion and using their slope as follows:

$$D = \pi\left(\frac{n}{4M_\infty}\right)^2\left(\frac{M_2 - M_1}{\sqrt{t_2} - \sqrt{t_1}}\right)^2$$

(18)

Using equation 18, a diffusivity constant can be determined for each experimental moisture sorption curve (as outlined in Section 3.3.3). From each replicate an average diffusivity per test condition can be calculated for each mix, and the predicted moisture sorption curve (versus time) can be plotted.

The goodness of fit of this model to the experimental data was assessed according to the correlation coefficient R^2 and the Root Mean Square Error (RMSE) [65]. The RMSE was calculated as follows in Equation 19:

$$RMSE = \sqrt{\frac{\sum_{i=1}^{n}(M_{water} - M_t)^2}{n}} \tag{19}$$

where M_{water} is the experimental moisture content (at any time t), M_t is the theoretical moisture content, and n is the number of observations.

4.0 Results and Discussion

4.1 Fiber and Composite Characterization

4.1.1 Fiber Fractionation and Size Distribution

Fractionation of fiber feedstocks (hammer milled hemp hurd and wheat straw) was performed using sieving methods in order to separate various particle sizes prior to composite manufacturing. Figure 4.1 summarizes the fraction of particle sizes retained in each sieve size for both fiber types. This analysis provides the particle size distribution of the feedstock material prior to size separation. While both fiber types were processed at different locations (and using different milling equipment), the resulting particle size distribution of the supplied fibers was quite similar.
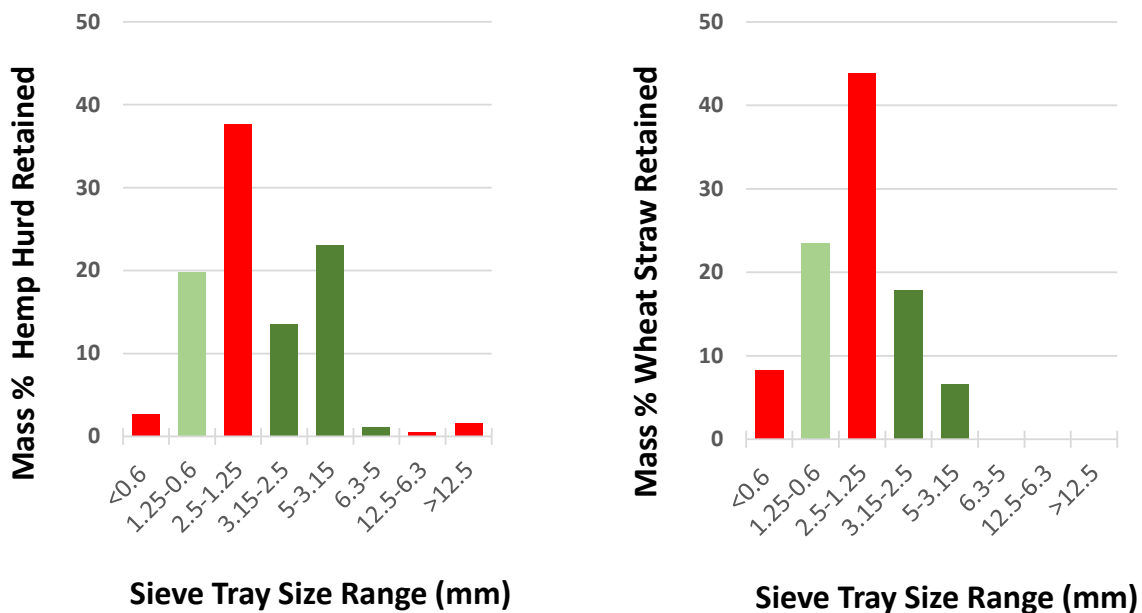

Figure 4.1 Particle size distribution of the feedstock fiber materials based on sieve shaker tray opening sizes: hemp hurd (left) and wheat straw (right) – groupings: coarse (dark green), fine (light green) and rejected (red)

The resulting sieved fibers were then grouped into two categories: 1). "Coarse" fiber group representing a size range 2.5 mm to 5 mm (i.e. all fibers that were retained on the 2.5 mm and 3.15 mm sieves), and 2). "Fine" fiber group representing a size range 0.6 mm to 1.25 mm (i.e. all fibers that were retained on the 0.6 mm sieve). These two groupings provide a distinguished separation in particle sizes (with no overlap), which were then used to prepare cement composite specimens to assess the effect of fiber particle size. Figure 4.2 shows the resulting fiber samples after fractionization grouped by size and fiber type. It is clear that there is a distinct difference in observed fiber length and fineness between the coarse and fine particle groupings. In general, wheat straw fibers tend to have a higher aspect ratios (particle length to width) compared to the hemp hurd fiber which appears more bulky (somewhat lower length to width ratio).

Surface photographs of these fibers types and sizes embedded in sanded fiber-cement composite specimens is also shown in Figure 4.3 for comparison. These images clearly show an observed difference in particle sizes between the coarse fiber, fine fiber and control (no fiber), as well as the increase in fiber quantity with increasing fiber volume fraction.

Figure 4.2: Fractionated fibers sizes used in this study

Figure 4.3: Manufactured thermal insulation test panels

4.1.2 Measured Fiber Densities

The fiber densities were determined prior to sample manufacturing, and were used to calculate required mixing ratios to achieve a target fiber volume fraction in the final composite specimens (as discussed in Section 3.2.2). Density results for each fiber type and size are shown in Table 4.1. Hemp hurd was found to have a higher overall density compared to wheat straw fibers. Both coarse and fine fiber fractions for hemp hurd had statistically similar density values, while fine wheat straw was seen to have a slightly higher density compared to the fine fraction.

Table 4.1: Mean particle densities determined using a nitrogen gas pycnometer; letters that do not share the same letter are significantly different (95% confidence interval, Tukey)

Fibers	Mean Particle Density (g/cm^3)
Fine Hemp Hurd	$1.46^a \pm 0.01$
Coarse Hemp Hurd	$1.50^a \pm 0.05$
Fine Wheat Straw	$1.05^b \pm 0.02$
Coarse Wheat Straw	$0.96^c \pm 0.03$

4.1.3 Pre-Mix Fiber Saturation Results

Water sorption data for the two fiber types and sizes prior to cement mixing (pre-soaking step) is shown Table 4.2. The purpose of this pre-soaking step is to prevent (or reduce) moisture uptake from the wet cement during cement hydration during fiber-cement mixing and curing. It can be seen that all fiber types and sizes have significant water uptake which is common in ligno-cellulosic materials. Wheat straw is observed to absorb more water than the hemp hurd, and the fine fiber sizes seems to absorb more than the coarse fractions. Since water saturation was performed by soaking and then draining the fiber mass, it is not surprising that the fine fiber fractions retained more water compared to the coarse group since fine fibers typically have larger available surface areas (i.e. more bonding sites for water).

Table 4.2: Mean water uptake in fibers during pre-mix soaking

Fibers	Mean Water Uptake in Fibers (% by mass)
Fine Hemp Hurd	259 ± 11
Coarse Hemp Hurd	168 ± 6
Fine Wheat Straw	341 ± 21
Coarse Wheat Straw	247 ± 5

4.1.4 Fiber-Cement Composite Densities

The bulk densities for each fiber composite combination (after manufacturing) were determined based on the specimen weight and volumetric dimensions. The plate specimens used for the thermal insulation tests were utilized for this purpose. The results are shown in Figure 4.4 for the various fiber types, fiber sizes and fiber volume fractions. Overall, it can be seen that the bulk density of the composites decrease with increasing fiber content, and all are lower than the measured density of the cement control (which is to be expected due to the low density nature of bio-based fibers compared to cement).

In terms for fiber type, the wheat straw composites had a slightly higher densities compared to the hemp hurd composites. This is likely due to differences in compaction effects during mixing. Wheat straw was found to be more brittle and easier to crush (relative to hemp hurd), and as a result, this would lead to a more compact dense composite material.

In terms of fiber size, the composites with coarse particles also had a slightly higher densities compared to the composites with fine particle sizes. According to Stevulova et al. [24] the composite pore size highly influences the density of the final product. The smaller pores introduced by the smaller fiber sizes allow for a denser binder structure and therefore increases the overall density of the composite samples.
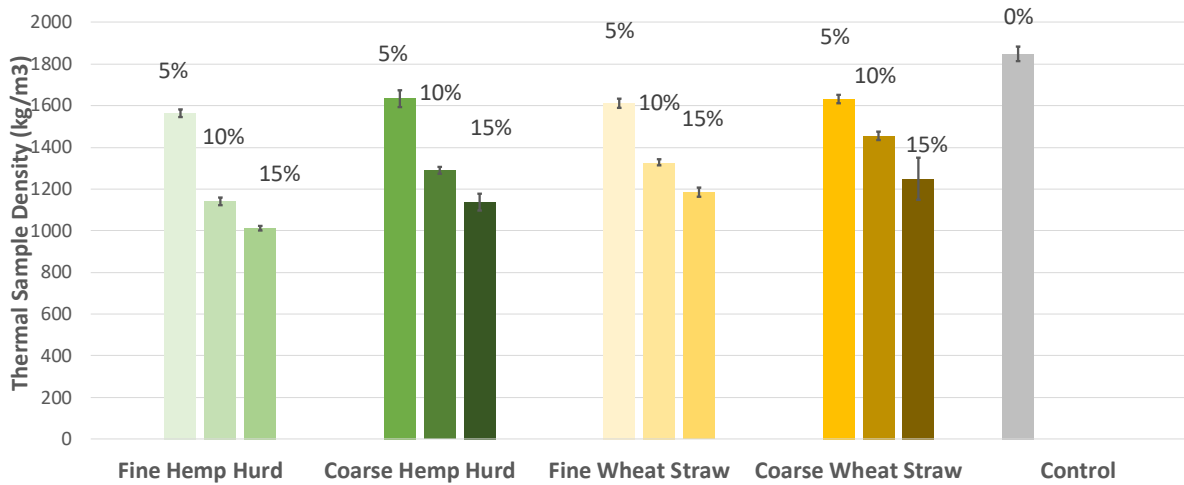
Figure 4.4: Bulk density of various hemp hurd and wheat straw based cement composites (error bars represent ± one standard deviation)

4.2 Compression Test Results

Compression tests were performed on the 13 unique natural fiber cement mixes to assess the effect of fiber type, fiber size, and fiber volume fraction. The results are shown in Figure 4.5. For all fiber composites tested, it can be seen that there is a general trend of decreasing compression strength with increasing fiber content (all fiber reinforced cements were significantly different from the control). Fiber volume fraction has the most significant effect compared to fiber type and size. In the case of fiber type, there was no statistical difference between the hemp hurd and wheat straw. This suggests that the compressive strength of the composite is mainly governed by the behaviour of the cement matrix rather than the fiber. It follows suit that the decrease in compressive strength with increasing fiber content is likely due

to the reduction in the overall amount of cement present in the composite (i.e. less cement, less compressive strength). The result between a decreasing compression strength and increasing fiber fraction is corroborated in studies with other natural fiber types Li et al., Murphy et al. and Stevulova et al. [60,61,64].

Conversely, fiber size displayed a small statistical difference with the fine fibers having a slightly higher average compression strength than the coarse fibers. This trend follows closely to the results presented by Stevulova et al. [24] in which the authors suggest that a smaller average particle size leads to finer pores therefore producing a stronger binder structure.
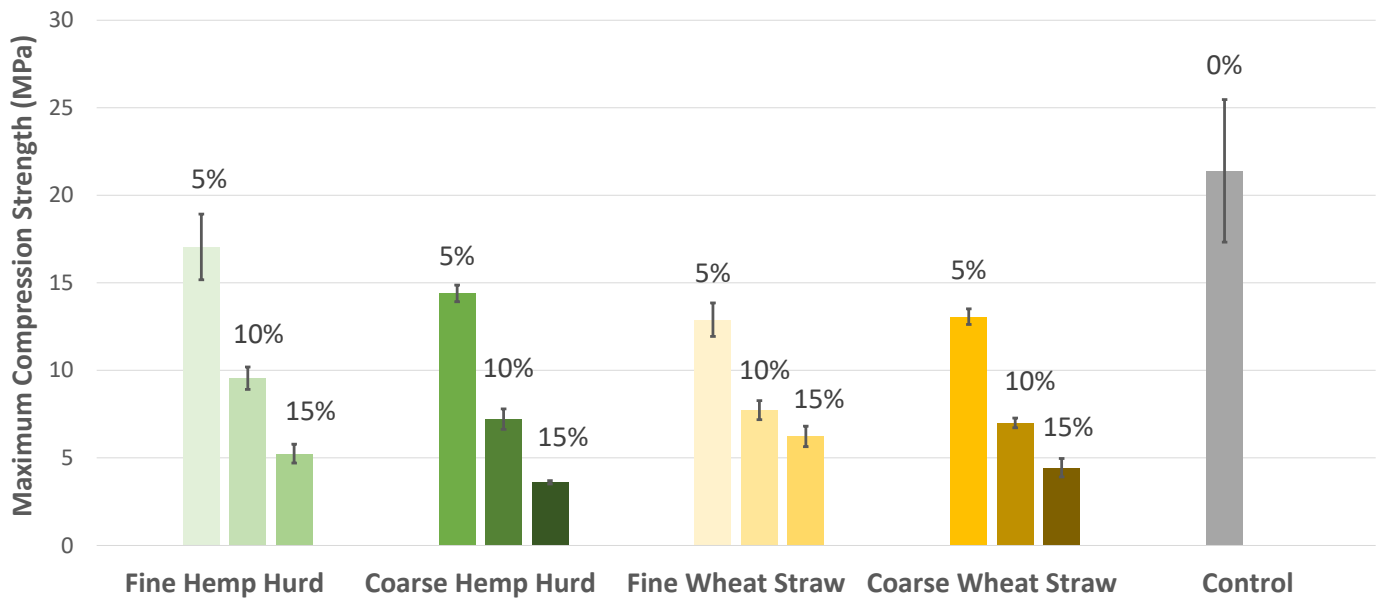

Figure 4.5: Compression strength of various hemp hurd and wheat straw based cement composites (error bars represent ± one standard deviation)

4.3 Flexural Test Results

Flexural test results for the 13 unique fiber cement mixes are shown in Figure 4.6. It can be seen that all fiber reinforced composites had higher flexural strengths compared to the unreinforced control (no fibers). Overall, the best fiber type/size combination was the fine wheat straw reinforced cement at a 10% fibre fraction (by volume), which increased the flexural strength by approximately 5 times compared to the unreinforced cement (control). These improvements in flexural strength were much larger than results found in the literature for similar fiber types [46]. Most of the flexural strength results seem to reach a peak at 10% fiber volume fraction then drop-off (in most cases). This is opposite to that found in the compressive strength tests which saw a decreasing strength with increasing fiber fraction. The fiber type also seems to play a more significant role in flexural properties compared to the compressive properties. All wheat straw combinations had significantly higher flexural strengths compared to their hemp hurd counterparts. Finally, there appears to be no consistent trend with respect to fiber size.

The improved flexural strength of all the fiber reinforced specimens is likely due to fiber bridging effects observed on the tensile side of the bend specimen. When bending load was applied to the control specimens (unreinforced cement), it was observed that the failure initiated on the tensile side of the bending sample resulting in an abrupt fracturing of the specimen. For the composite specimens, the fiber reinforcement delayed the onset and severity of tensile cracking during the test due to fiber bridging which resulted in a higher applied load (or stress) at failure. This bridging effect may also explain why wheat straw performed better than hemp

hurd in this loading mode. From Figure 4.2, it can be seen that the wheat straw fibers have a higher aspect ratio compared to the hemp hurd. This higher aspect ratio likely resulted in an improved fiber pull out strength which enhances the fiber bridging effect. While the fiber pull-out properties were not specifically assessed in this work, there have been a number of studies using other fiber types which have suggested this mechanism [69,70]. In terms of the noted drop in flexural strength after 10% volume fraction (for most mixes), the mechanism could possibly be attributed to the diminishing strength on the compressive side of the bend specimen (i.e. an increase in fiber content decreases the compressive strength as noted in section 4.2). This highlights the unique balance between tensile and compressive properties in bending applications.
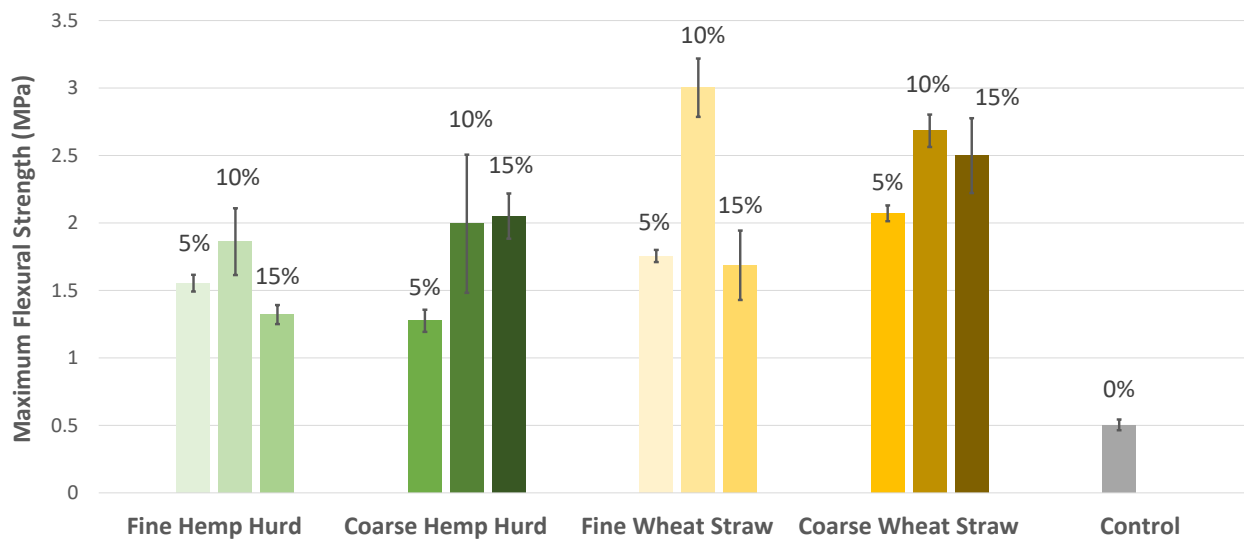

Figure 4.6: Flexural strength of various hemp hurd and wheat straw based cement composites (error bars represent ± one standard deviation).

4.4 Thermal Insulation Test Results

Results from the thermal insulation tests for both the hemp hurd and wheat straw composites are shown in Figure 4.7. All composite plates tested had an average moisture content of 12.9 ± 0.7% while the control specimens had an average moisture content of 11.3 ± 0.4% (all after 3 months conditioning in the lab). From Figure 4.7, it can be seen that the fiber volume fraction plays a significant role in improving thermal resistance in the cement composite. In general, the mean thermal resistance (R-Value per inch) increases with increasing fiber content. In addition, all fiber composites at 15% fiber fraction (by volume) provided approximately double the R-value compared to the unreinforced cement (control). This increase in thermal resistance in the composites is due to the lower thermal conductivity of natural fibers relative to the cement matrix [21].

In terms of fiber type and size, there was no significant difference between the groups. This is in contrast to results found by Stevulova et al. [24] who investigated the thermal resistance of hemp hurd composites. According to this study, the pore sizes within the composite were found to greatly influence the thermal insulation capacity of the final product (i.e. greater the pore size, the greater the thermal resistance). The smaller pores introduced by fine or smaller fiber sizes result in a denser binder structure, and therefore decrease the thermal resistivity of the samples. For the current study, this trend was not observed. However, it should be noted that the results for the thermal insulation tests showed high variability which may have ultimately hampered the ability to discern fibre size trends.
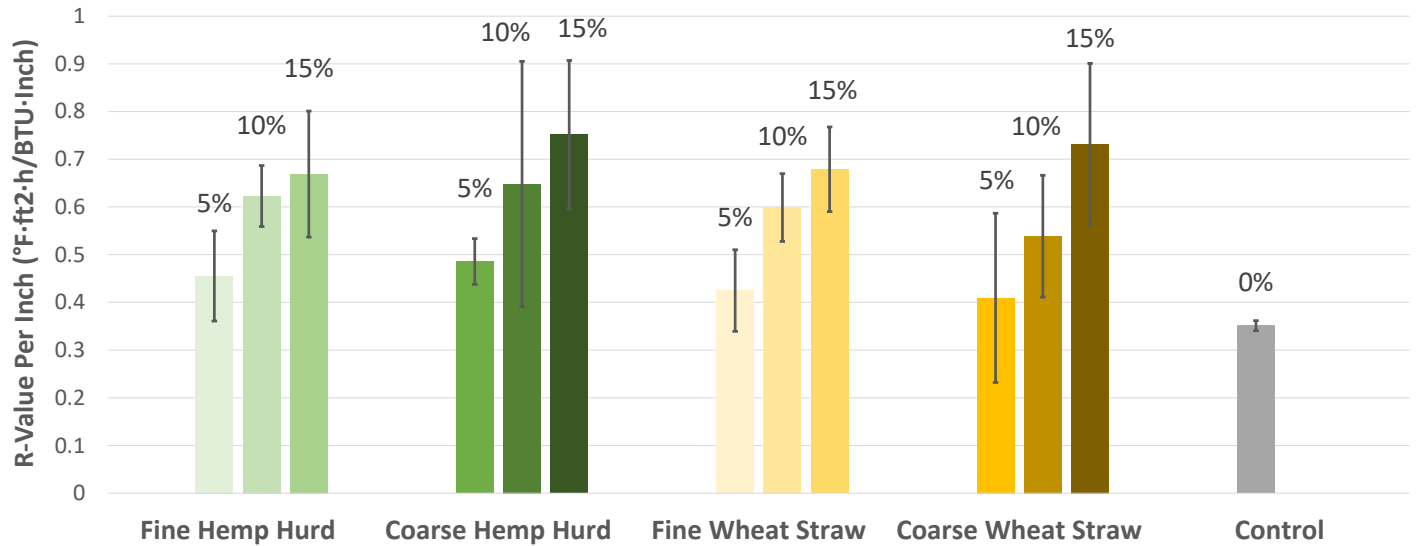
Figure 4.7: Thermal insulation values of various hemp hurd and wheat straw based cement composites (error bars represent ± one standard deviation).

Since material density plays a significant role in thermal conduction, the relationship between the resulting thermal resistivity (R-Value per in) and the densities of the thermal specimens (taken from Figure 4.4) were plotted against one another, and are shown in figure 4.8. It can be seen that as the density of the composites increases, the resulting thermal resistivity (R-Value per in) decreases. At higher fiber volume fractions, the spread of the data is greater than at lower volume fractions. This large variation in results at high fiber fractions may be due to difficulties in obtaining a homogeneous mix when larger amount of fibers is introduced. The resulting inhomogeneity could significantly affect the consistency of thermal resistivity tests in plate type specimens.
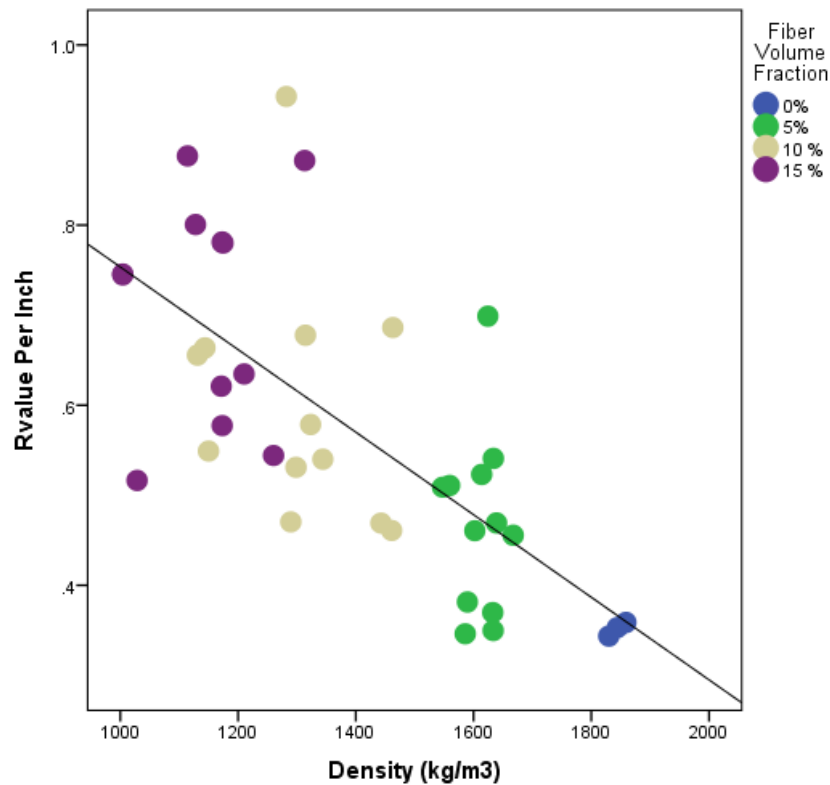
Figure 4.8: R-Value per inch of composites as a function of composite density

4.5 Water Sorption Test Results

The water sorption behaviour of the 13 unique natural fiber cement mixes was assessed to determine the performance of these materials when exposed to wet conditions (e.g. outdoor). The change in moisture content of specimens exposed to water over time was investigated for each fiber type, fiber size and fiber volume fraction. The moisture sorption curves for coarse wheat straw, fine wheat straw, coarse hemp hurd and fine hemp hurd are shown in Figures 4.9 thru 4.12, respectively. For each of these graphs, both the short-term (1

hour) and longer-term responses (3 days) are provided for the different fiber fractions along with predicted responses from the Fickian diffusion model [64] as outlined in Section 3.4.

Referring to Figure 4.9, it can be seen that a majority of water is absorbed within the first hour of exposure (see Figure 4.9a). As time increases, this sorption rate decreases until a plateau (or saturation) in the moisture content is achieved (see Figure 4.9b). Fiber fraction is shown to have a significant effect on the moisture response curves. As the fiber fraction increased, so did the moisture sorption rate (initial slope of the moisture-time response) and the saturation moisture content (M_∞). The unreinforced cement had the lowest saturation moisture content at 19.4%, while the 15% coarse wheat straw composite had the saturation moisture content at 34.5%. Both the unreinforced and reinforced cement samples were seen to absorb water which suggests that a combination of porosity within the cement matrix and the hydrophillic fibers were both responsible for mass transport into the specimens.

In addition to the experimental results, the predicted responses from the Fickian model is also plotted in Figures 4.9a and 4.9b for each fiber fraction. The model provides a reasonable prediction of the moisture content at both the initial immersion period (from 0 to 5 min.) and at longer times ($\geq$ 1 day), but seems to overestimate the moisture sorption at periods in between. Overall, both the experimental and predicted moisture sorption curves for the other fiber types and sizes (Figures 4.10-4.12) follow the same general trends.

In order to simplify the comparison between fiber types and sizes, the mean diffusivity (which represents the initial moisture-time response rate as derived in Section 3.4) and the saturation moisture content (based on the experimental results) was tabulated in Table 4.3 for

each mix configuration. In addition, Table 4.3 also displays the correlation coefficient (R^2) and

RMSE which measures the "Goodness of Fit" between the experimental data and the

theoretical model.

Referring to Table 4.3, fiber volume fraction had the greatest effect on moisture

sorption response compared to both fiber type and size. In general, samples with a higher fiber

content displayed a higher saturation moisture content (M_∞). However, there was no

discernable trend for the diffusivity values for all composite specimens. In terms of fiber type,

the hemp hurd composites had slightly higher mean saturation moisture contents relative to

the wheat straw composites. Specimens with the fine fiber sizes also had a slightly higher mean

saturation moisture contents compared to specimens with the coarse fiber size. This result is

consistent with the observations reported in Stevulova et al. [49]. A possible explanation for

this behavior is that the smaller particle sizes result in a larger number of individual particles

within the composite. These particles have a larger total surface area therefore creating more

accessible pathways that allow for more water absorption.

For the control specimens (unreinforced cement), the saturation moisture content was

lower than that of the fiber composite samples, however, the diffusivity values greater. This

higher diffusion rate for the control versus the fiber composites could be explained by possible

differences in surface features in the materials. The presence of pores on the surface of the

cement would allow a faster sorption rate through capillary action versus the slower diffusion

of water via ligno-cellulosic fibers. However, since the moisture content at saturation is

governed by interconnectivity of pores or fibers in a system, it would indicate that the pores in

unreinforced cement are not well connected. For the fiber composites, this saturation moisture

level increases as fiber content (and associated connectivity) increases. The relative uniformity

of the diffusivity value for all composite samples suggests that the initial water sorption rate is

somewhat random depending on the number of accessible fibers on the surface of the

specimens (rate limiting factor).

In terms of Fickian model predictions, the theoretical curves are reasonable fit of the

experimental data. However, these curves see some deviation with increasing fiber volume

fraction, and is greatest in the hemp hurd samples (see Figure 4.11 and 4.12). This suggests that

these mixes exhibit a dual phase moisture absorption mechanism similar to *Raphia vinifera*

fibers studied by Mbou et al. [65]. Sinka et al. [62] also found that hemp hurd exhibits a two-

phase diffusion mechanism. This is the result of the combination of capillary action following

Fick's law, and the occurrence of hydroxyl groups and amorphous areas in the cellulose within

the hemp. Additionally, since hemp hurd has a larger proportion of cellulose than wheat straw,

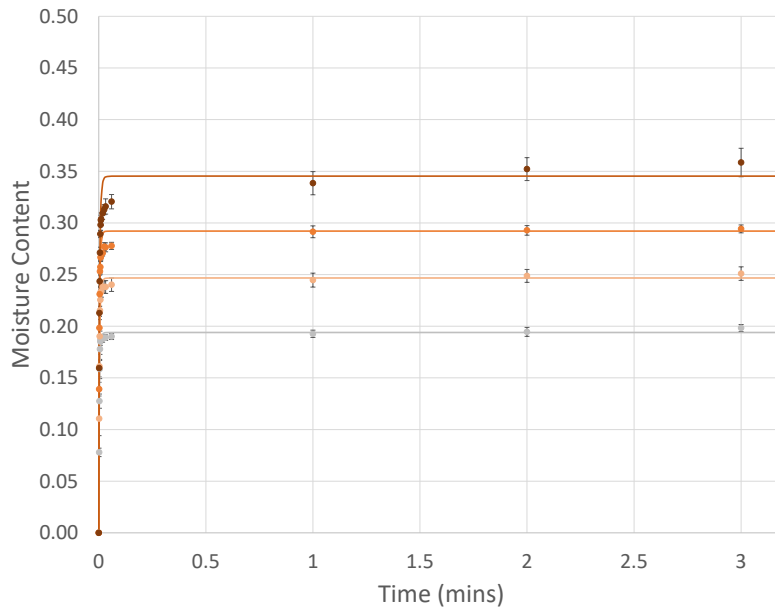it is expected that the hemp hurd samples would absorb more water.

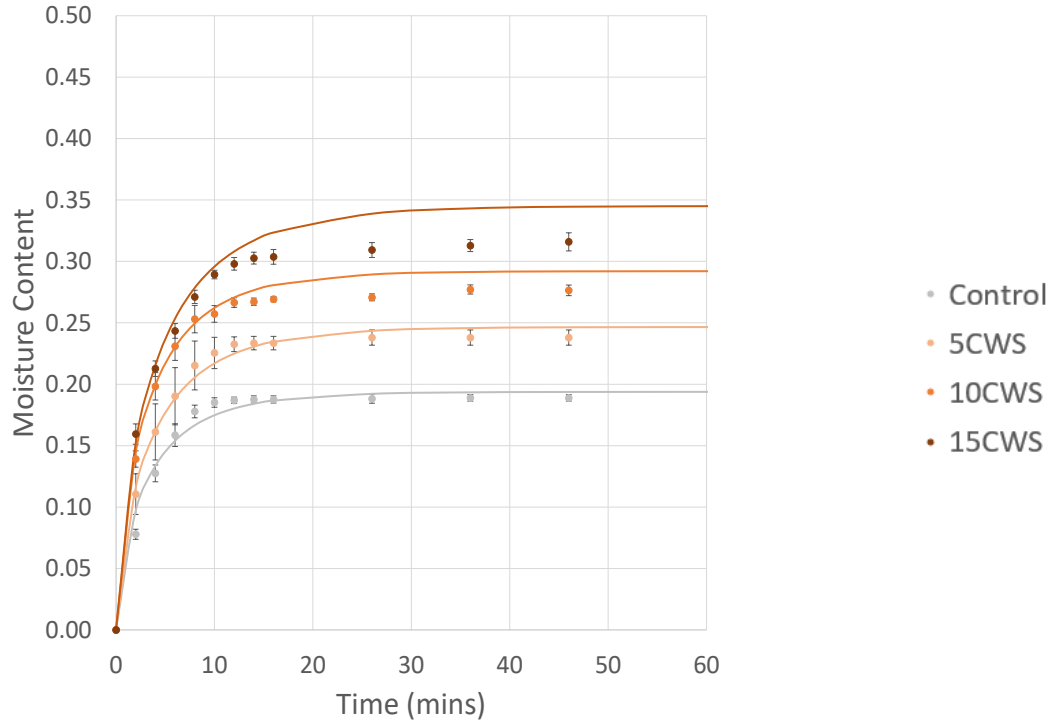*Figure 4.9: Experimental and predicted (solid line) water sorption behavior of coarse wheat straw composites and the unreinforced control: a). short-term response (top), and b). long-term response (bottom). Error bars represent ± one standard deviation.*
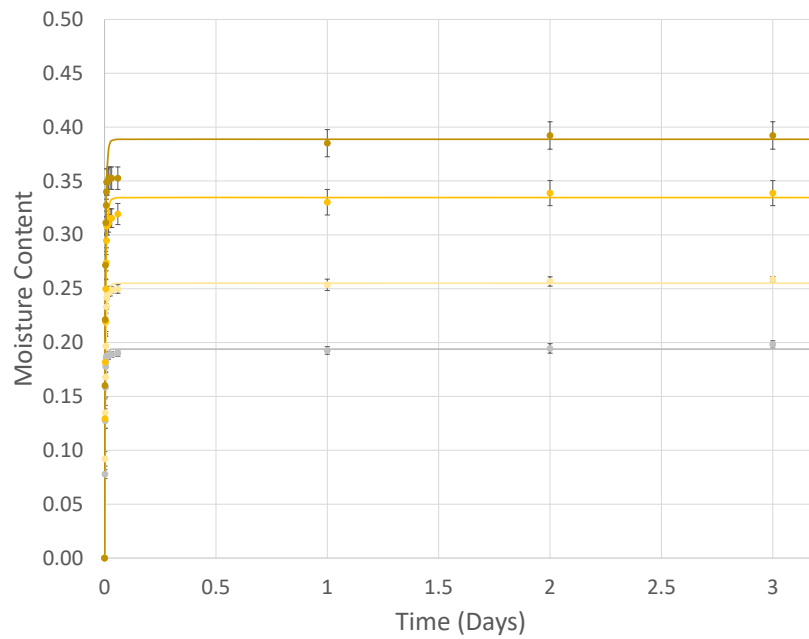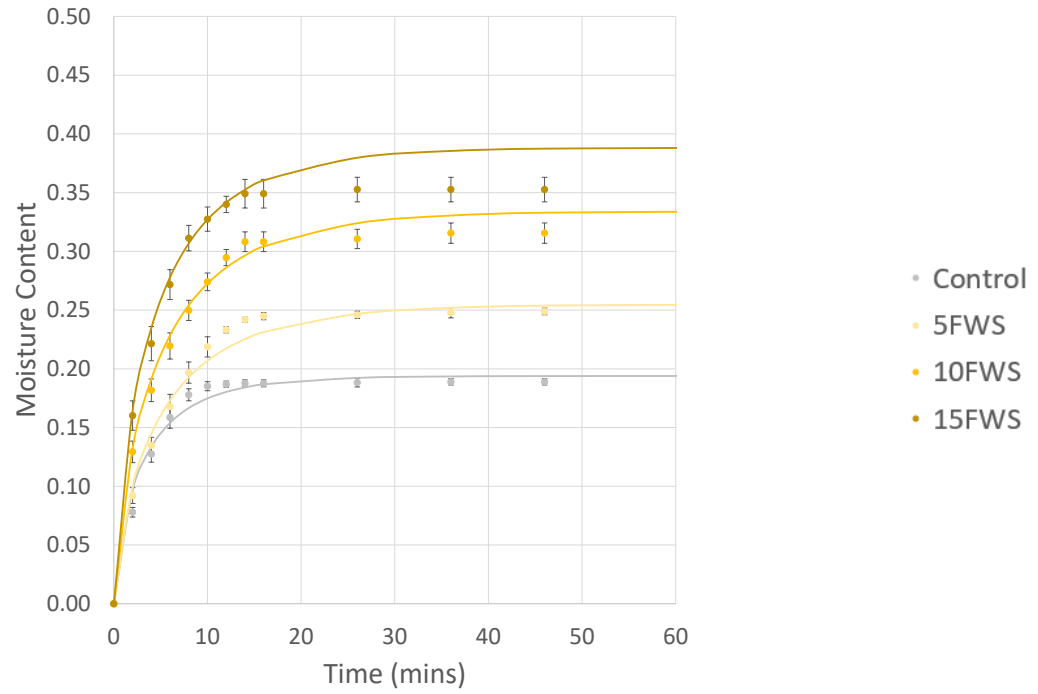
Figure 4.10: Experimental and predicted (solid line) water sorption behavior of fine wheat straw composites and the unreinforced control: a). short-term response (top), and b). long-term response (bottom). Error bars represent ± one standard deviation.

Figure 4.11: Experimental and predicted (solid line) water sorption behavior of coarse hemp hurd composites and the unreinforced control: a). short-term response (top), and b). long-term response (bottom). Error bars represent ± one standard deviation.
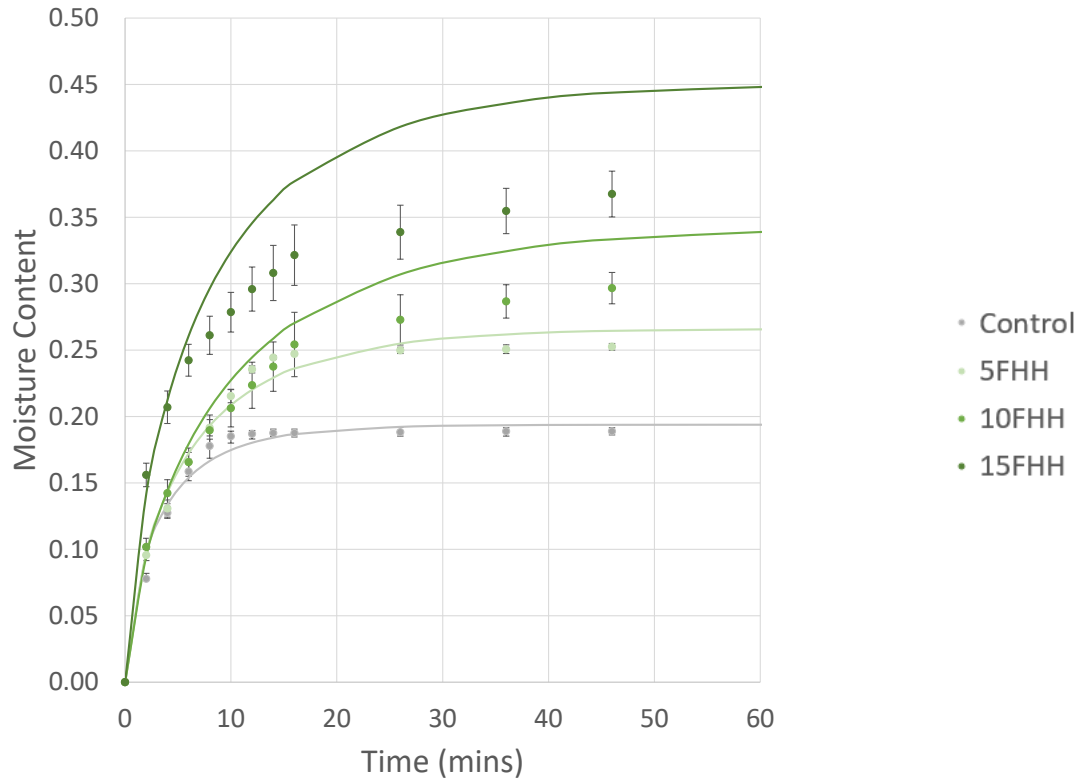
Figure 4.12: Experimental and predicted (solid line) water sorption behavior of fine hemp hurd composites and the unreinforced control: a). short-term response (top), and b). long-term response (bottom). Error bars represent ± one standard deviation.
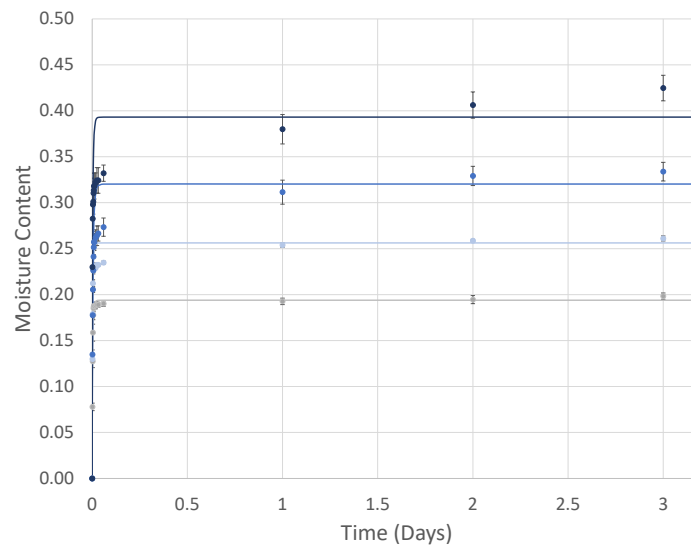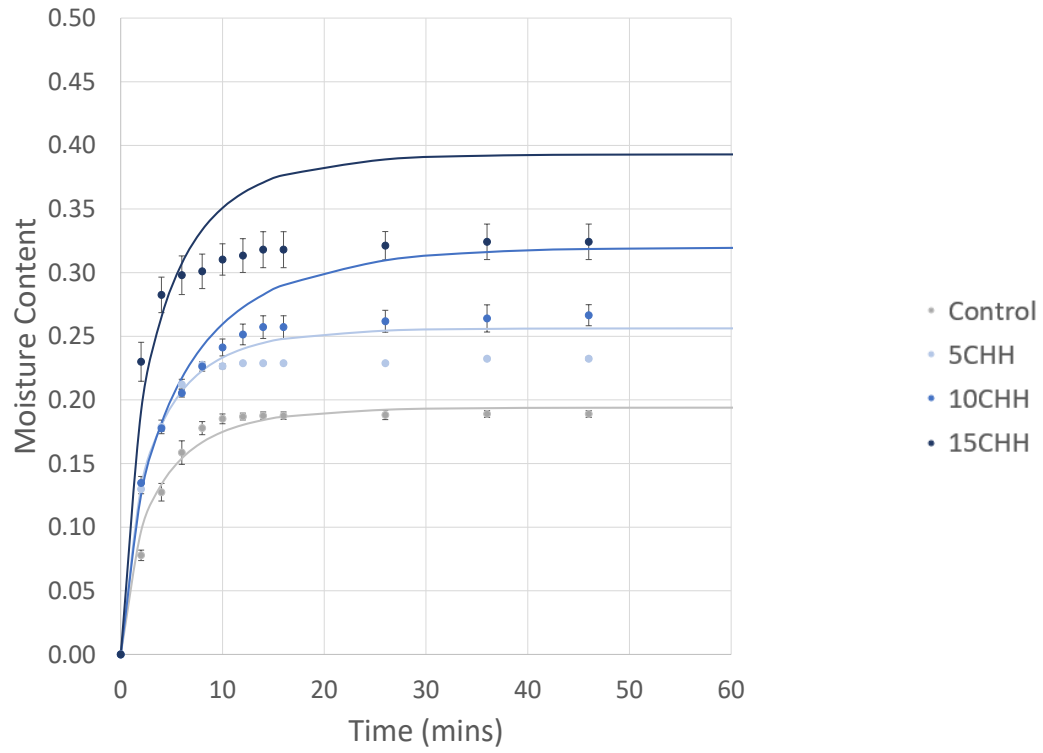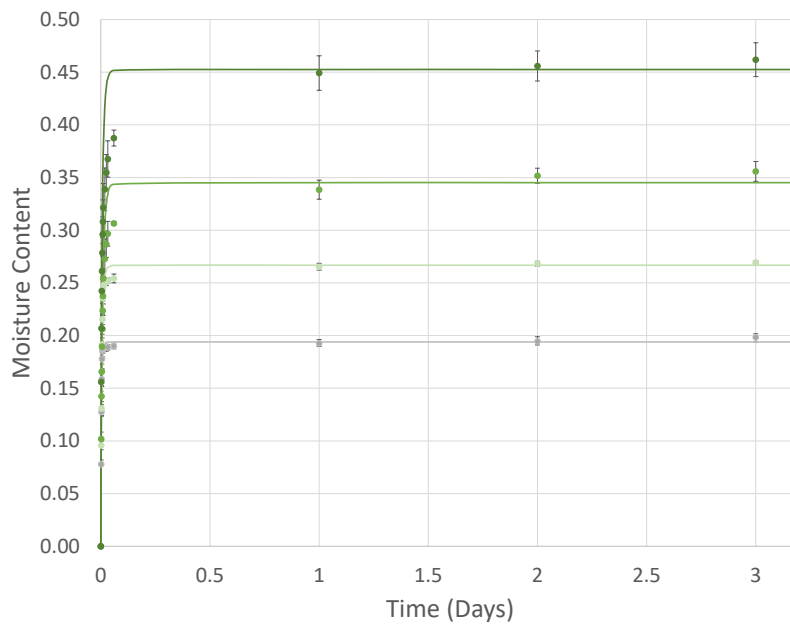
Table 4.3 – Summary of Moisture Sorption and Model Fit Parameters

Fiber Type	Fiber Size	Fiber Volume Fraction	Specimen Number	*D* Diffusivity (mm²/min)	M_∞ Saturation Moisture Content (%)	Goodness of Fit (R²)	Goodness of Fit (RMSE)
Cement Only	----	----	Control	10.48	19.4	0.990	0.008
Hemp Hurd	Fine	5	5FHH	4.23	26.7	0.992	0.009
		10	10FHH	2.13	34.5	0.980	0.023
		15	15FHH	3.84	45.3	0.952	0.048
	Coarse	5	5CHH	4.35	25.6	0.982	0.014
		10	10CHH	4.22	32.0	0.951	0.030
		15	15CHH	4.54	39.3	0.911	0.046
Wheat Straw	Fine	5	5FWS	4.15	25.5	0.993	0.009
		10	10FWS	3.86	33.5	0.995	0.010
		15	15FWS	2.45	38.9	0.988	0.018
	Coarse	5	5CWS	4.45	24.7	0.996	0.006
		10	10CWS	3.38	29.2	0.993	0.010
		15	15CWS	5.82	34.5	0.986	0.017

5.0 Conclusions

This study outlines the assessment of mechanical, thermal insulation, and water absorption behaviour of various natural fiber reinforced Portland cement composites. The purpose of the study was to assess property ranges for these renewable composite options which can provide useful data in engineering design. Specimens were successfully manufactured using two fiber types (hemp hurd and wheat straw) sieved into two fiber size ranges (a "coarse" group based on 2.5 – 5 mm particle sizes; and a "fine" group based on 0.6 – 1.25 mm particle sizes). Cylindrical (compression), beam (flexural) and plate (insulation and moisture sorption) samples were then manufactured using 3 fiber volume fractions (5%, 10%, and 15%) and a control (unreinforced cement).

In terms of compression test results, the addition of natural fibers to the cement resulted in lower compression strengths compare to the control. As the fiber content was increased, the compression strength decreased. Fiber size had a small effect with fine fiber sample having a slightly higher average compression strength compared to the coarse fiber group. In the case of fiber type, there was no statistical difference between the hemp hurd and wheat straw in terms of composite compressive properties.

For the flexural properties, the addition of natural fibers to cement increased the flexural strength of the cement by up to 5 times for the mix combinations studied. As fiber content was increased, the flexural strength results seem to reach a peak at 10% fiber volume fraction then drop-off (in most cases). This plateau effect was attributed to the interplay of the controlling failure mechanisms. As the fiber fraction increases, the fiber bringing effect on the tensile side of

the flexural specimen is improved, however, the strength on the compressive side of the flexural specimen decreases. In terms of fiber types, the wheat straw composites had higher flexural strengths compared to the hemp hurd specimens. However, there were no consistent trend with respect to fiber size.

The addition of fibers was also observed to significantly increase the insulative properties of cement by up to 65% for the mix combinations studied. This increase in thermal resistivity is attributed to the good insulating properties of the lignocellulosic fibers. While increasing fiber fraction had the most significant effect on R-Value, the effect of fiber type and size was not significant.

The amount of moisture uptake in cement also increased with the addition of natural fibers by up to 125% for the mix combinations investigated. Fiber fraction had the biggest effect on moisture sorption. As fiber content was increased, there was a corresponding increase in saturation moisture content. Both fiber type and size were also found to affect moisture behavior, however, these effects were not a significant as fiber fraction. Hemp hurd composites had slightly higher saturation moisture contents relative to the wheat straw composites, while specimens with the fine fiber size had slightly higher saturation moisture contents compared to specimens with the coarse fiber size.

A model developed by Shen and Springer [64] for moisture sorption in composite plates was used to predict the moisture response of the composite an control samples tested. Overall, the model demonstrated a reasonable fit to the experimental data except at the point where the moisture sorption curve begins to plateau. At this region of the curve, the model is seen to

overshoot the experimental data suggesting a two-phase diffusion mechanism may be present (i.e. a combination of capillary and diffusion mechanisms). This discrepancy was more significant for the hemp hurd composite results.

In general, this study demonstrated that cements reinforced with natural fibers offer improved flexural (crack resistance) and insulating properties compared to unreinforced cement which may be advantageous in a number of building product applications. However, these natural fiber composites also had reduced compressive strengths, and were more susceptible to moisture sorption which may limit their use to non-structural applications. If these materials are to use in outdoor applications, a protection strategy against moisture ingress (e.g. coating) would also need to be considered. Even with these limitations, however, there is still considerable market opportunities as an insulating material which can also reduce cracking in cementous binders. That being said, this study has demonstrated an effective option to improve the sustainability of cement materials by using renewable content.

6.0 Novelty of work and future research

This work has investigated a unique set of variables that affect the performance and viability of this innovative type of sustainable material. It is aimed to assist engineers and designers in understanding the practicality and limitations of natural fiber cement composites for building applications. Feedstocks selected in this study are readily produced in Western Canada, and may offer future revenue streams for agricultural producers. Future studies

extending from this work should focus on the practical assessment of workability of hemp based cements and the effect of water-cement ratios.

Further research is also recommended to fully understand the mechanisms at work. Microscopy could help better explain the fiber-cement bonding characteristics, and structures that are thought to be the causes of observed thermal and water sorption behaviours (i.e. inherent porosity and fiber structures in the cements). Unfortunately, this examination could not be completed as part of the current study due to the COVID-19 pandemic.

Additionally, further in-depth modeling of moisture sorption would allow to better understand the long-term water sorption behaviour, and the effect of moisture on mechanical and thermal resistivity over time. Finally, a life cycle assessment should be conducted to determine the environmental impact of these natural fiber-cement composites compared to unreinforced cements and concretes.

References:

[1] Morel, J., Mesbah, A., Oggero, M., & Walker, P. (2001). Building houses with local materials: Means to drastically reduce the environmental impact of construction. *Building and Environment, 36*(10), 1119-1126.

[2] *Green building in Canada assessing the market impacts & opportunities.* https://www.cagbc.org/CAGBC/Advocacy/Green_Building_in_Canada_Assessing_the_Market_Impacts_Opportunities.aspx

[3] Kurad, R., Silvestre, J. D., de Brito, J., & Ahmed, H. (2017). Effect of incorporation of high volume of recycled concrete aggregates and fly ash on the strength and global warming potential of concrete. *Journal of Cleaner Production, 166*, 485-502.

[4] Andrew, R. M. (2018). Global CO 2 emissions from cement production. *Earth System Science Data, 10*(1), 195-217.

[5] Worrell, E., Price, L., Martin, N., Hendriks, C., & Meida, L. O. (2001). Carbon dioxide emissions from the global cement industry 1. *Annual Review of Energy and the Environment, 26*(1), 303-329. doi:10.1146/annurev.energy.26.1.303

[6] Statistics Canada. Table 001-0041 - Supply and disposition of grains in Canada as of March 31, July 31, August 31 (soybeans only) and December 31, occasional (metric tonnes), CANSIM (database). https://doi.org/10.25318/3210001301-eng (accessed:29-05-2018)

[7] Statistics Canada. Table 32-10-0359-01 - Estimated areas, yield, production, average farm price and total farm value of principal field crops, in metric and imperial units, occasional (metric tonnes), CANSIM (database). https://doi.org/10.25318/3210035901-eng (accessed:15-03-2021)

[8] Aubin, M.-P., Seguin, P., Vanasse, A., Lalonde, O., Tremblay, G.F., Mustafa, A.F., & Charron, J-B. (2016). Evaluation of eleven industrial hemp cultivars grown in eastern Canada. *Agronomy, 108*(5), 1972-1980.

[9] Rudin, A., Choi, P., Rudin, A., Aegerter, M. A., Leventis, N., & Koebel, M. M. (2013). The elements of polymer science and engineering. Waltham, Mass.: Academic, 2013.., , 521-535.

[10] Banthia, N., Bentur, A., & Mufti, A. A. (1998). Fiber reinforced concrete: Present and future Canadian Society for Civil Engineering.

[11] Zollo, R. F. (1997). Fiber-reinforced concrete: An overview after 30 years of development. Cement and Concrete Composites, 19(2), 107-122. doi:https://doi.org/10.1016/S0958-9465(96)00046-7

[12] Egyptology, & , V. L. (2009). UCLA UCLA encyclopedia of egyptology title mud-brick permalink journal UCLA encyclopedia of publication date

[13] Mohanty, A. K., Misra, M. a., & Hinrichsen, G. I. (2000). Biofibres, biodegradable polymers and biocomposites: An overview. Macromolecular Materials and Engineering, 276(1), 1-24.

[14] Zhou, X. M., Madanipour, R., & Ghaffar, S. (2016). Impact properties of hemp fibre reinforced cementitious composites. Key Engineering Materials, 711, 163-170. https://doi.org/10.4028/www.scientific.net/kem.711.163

[15] Stevulova, N., Schwarzova, I., Hospodarova, V., & Junak, J. (2016). Implementation of waste cellulosic fibres into building materials. Chemical Engineering Transactions, 50, 367-372

[16] Snoeck, D., Smetryns, P.-A., & De Belie, N. (2015). Improved multiple cracking and autogenous healing in cementitious materials by means of chemically-treated natural fibres. Biosystems Engineering, 139, 87-99. https://doi.org/10.1016/j.biosystemseng.2015.08.007

[17] de Bruijn, P. B., Jeppsson, K.-H., Sandin, K., & Nilsson, C. (2009). Mechanical properties of lime-hemp concrete containing shives and fibres. Biosystems Engineering, 103(4), 474-479. https://doi.org/10.1016/j.biosystemseng.2009.02.005

[18] Merta, I., & Tschegg, E. K. (2013). Fracture energy of natural fibre reinforced concrete. Construction and Building Materials, 40, 991-997. https://doi.org/10.1016/j.conbuildmat.2012.11.060

[19] Walker, R., Pavia, S., & Mitchell, R. (2014). Mechanical properties and durability of hemp-lime concretes. Construction and Building Materials, 61, 340-348. https://doi.org/10.1016/j.conbuildmat.2014.02.065

[20] Jarabo, R., Fuente, E., Monte, M. C., Savastano, H., Mutjé, P., & Negro, C. (2012). Use of cellulose fibres from hemp core in fibre-cement production. Effect on flocculation, retention, drainage, and product properties. Industrial Crops and Products, 39, 89-96. https://doi.org/10.1016/j.indcrop.2012.02.017

[21] Awwad, E., Mabsout, M., Hamad, B., Farran, M. T., & Khatib, H. (2012). Studies on fiber-reinforced concrete using industrial hemp fibers. Construction and Building Materials, 35, 710-717. https://doi.org/10.1016/j.conbuildmat.2012.04.119

[22] Li, Z., Wang, X., & Wang, L. (2006). Properties of hemp fibre reinforced concrete composites. Composites Part A: Applied Science and Manufacturing, 37(3), 497-505. https://doi.org/10.1016/j.compositesa.2005.01.032

[23] Ferreira, S. R., de Andrade Silva, F., Lima, P. R. L., & Toledo Filho, R. D. (2015). Effect of fibre treatments on the sisal fiber properties and fiber-matrix bond in cement based systems. Construction and Building Materials, 101, 730-740. https://doi.org/10.1016/j.conbuildmat.2015.10.120

[24] Stevulova, N., Kidalova, L., Cigasova, J., Junak, J., Sicakova, A., & Terpakova, E. (2013). Lightweight composites containing hemp hurds. Procedia Engineering, 65, 69-74. https://doi.org/10.1016/j.proeng.2013.09.013

[25] Diquélou, Y., Gourlay, E., Arnaud, L. & Kurek, B. (2016). Influence of binder characteristics on the setting and hardening of hemp lightweight concrete. Construction and Building Materials, 112, 506-517. https://doi.org/10.1016/j.conbuildmat.2016.02.138

[26] Merta, I. (2016). Hemp fibres—A promising reinforcement for cementitious materials. In Fangueiro R., Rana S. (eds.), Natural Fibres: Advances in Science and Technology Towards Industrial Applications (pp. 291-303). Springer, Dordrecht. https://doi.org/10.1007/978-94-017-7515-1_22

[27] Balčiūnas, G., Pundienė, I., Lekūnaitė-Lukošiūnė, L., Vėjelis, S., & Korjakins, A. (2015). Impact of hemp shives aggregate mineralization on physical-mechanical properties and structure of composite with cementitious binding material. Industrial Crops and Products, 77, 724-734. https://doi.org/10.1016/j.indcrop.2015.09.011

[28] Diquélou, Y., Gourlay, E., Arnaud, L., & Kurek, B. (2015). Impact of hemp shiv on cement setting and hardening: Influence of the extracted components from the aggregates and study of the interfaces with the inorganic matrix. Cement and Concrete Composites, 55, 112-121. https://doi.org/10.1016/j.cemconcomp.2014.09.004

[29] Awwad, E., Hamad, B., Mabsout, M., & Khatib, H. (2014). Structural behavior of simply supported beams cast with hemp-reinforced concrete. ACI Structural Journal, 111(6), 1307-1316. https://doi.org/10.14359/51687032

[30] Li, Z., Wang, L., & Wang, X. (2004). Compressive and flexural properties of hemp fiber reinforced concrete. Fibers and Polymers, 5(3), 187-197. https://doi.org/10.1007/bf02902998

[31] Gourlay, E., Glé, P., Marceau, S., Foy, C., & Moscardelli, S. (2017). Effect of water content on the acoustical and thermal properties of hemp concretes. Construction and Building Materials, 139, 513-523. https://doi.org/10.1016/j.conbuildmat.2016.11.018

[32] Awwad, E., Mabsout, M., Hamad, B., & Khatib, H. (2011). Preliminary studies on the use of natural fibers in sustainable concrete. Lebanese Science Journal, 12(1), 109-117.

[33] Sedan, D., Pagnous, C., Smith, A., & Chotard, T. (2008). Mechanical properties of hemp fibre reinforced cement: Influence of the fibre/matrix interaction. Journal of the European Ceramic Society, 28(1), 183-192. https://doi.org/10.1016/j.jeurceramsoc.2007.05.019

[34] Arnaud, L., & Gourlay, E. (2012). Experimental study of parameters influencing mechanical properties of hemp concretes. Construction and Building Materials, 28(1), 50-56. https://doi.org/10.1016/j.conbuildmat.2011.07.052

[35] Raut, S. P., Ralegaonkar, R. V., & Mandavgane, S. A. (2011). Development of sustainable construction material using industrial and agricultural solid waste: A review of waste-create bricks. Construction and Building Materials, 25(10), 4037-4042. https://doi.org/10.1016/j.conbuildmat.2011.04.038

[36] Muda, Z. C., Kamal, N. L. M., Syamsir, A., Sheng, C. Y., Beddu, S., Mustapha, K. N., et al. (2016). Impact resistance performance of kenaf fibre reinforced concrete. Paper presented at the IOP Conference Series: Earth and Environmental Science, , 32. (1) pp. 012019.

[37] Elsaid, A., Dawood, M., Seracino, R., & Bobko, C. (2011). Mechanical properties of kenaf fiber reinforced concrete. Construction and Building Materials, 25(4), 1991-2001. https://doi.org/10.1016/j.conbuildmat.2010.11.052

[38] Wei, J., & Meyer, C. (2015). Degradation mechanisms of natural fiber in the matrix of cement composites. Cement and Concrete Research, 73, 1-16. https://doi.org/10.1016/j.cemconres.2015.02.019

[39] Wei, J., & Meyer, C. (2014). Improving degradation resistance of sisal fiber in concrete through fiber surface treatment. Applied Surface Science, 289, 511-523. https://doi.org/10.1016/j.apsusc.2013.11.024

[40] Page, J., Sonebi, M., & Amziane, S. (2017). Design and multi-physical properties of a new hybrid hemp-flax composite material. Construction and Building Materials, 139, 502-512. https://doi.org/10.1016/j.conbuildmat.2016.12.037

[41] Bledzki, A. K., & Gassan, J. (1999). Composites reinforced with cellulose based fibres. Progress in Polymer Science, 24(2), 221-274. https://doi.org/10.1016/s0079-6700(98)00018-5

[42] Akil, H., Omar, M. F., Mazuki, A. M., Safiee, S., Ishak, Z. M., & Bakar, A. A. (2011). Kenaf fiber reinforced composites: A review. Materials & Design, 32(8-9), 4107-4121. https://doi.org/10.1016/j.matdes.2011.04.008

[43] Cigasova, J., Stevulova, N., & Junak, J. (2014). Innovative use of biomass based on technical hemp in building industry. Chemical Engineering Transactions, 37

[44] Diquélou, Y., Gourlay, E., Arnaud, L., & Kurek, B. (2015). Impact of hemp shiv on cement setting and hardening: Influence of the extracted components from the aggregates and study of the interfaces with the inorganic matrix. Cement and Concrete Composites, 55, 112-121. https://doi.org/10.1016/j.cemconcomp.2014.09.004

[45] Nazerian, M., & Sadeghiipanah, V. (2013). Cement-bonded particleboard with a mixture of wheat straw and poplar wood. Journal of Forestry Research, 24(2), 381-390. https://doi.org/10.1007/s11676-013-0363-8

[46] Sedan, D., Pagnoux, C., Smith, A., & Chotard, T. (2008). Mechanical properties of hemp fibre reinforced cement: Influence of the fibre/matrix interaction. Journal of the European Ceramic Society, 28(1), 183-192. https://doi.org/10.1016/j.jeurceramsoc.2007.05.019

[47] A. K. Mohanty, M. Misra & L. T. Drzal (2001) Surface modifications of natural fibers and performance of the resulting biocomposites: An overview, Composite Interfaces, 8:5, 313-343, DOI: 10.1163/156855401753255422

[48] Stevulova, N., Cigasova, J., Purcz, P., & Schwarzova, I. (2014). Long-term water absorption behaviour of hemp hurds composites. Chemical Engineering, 39, 559-564.

[49] Stevulova, N., Cigasova, J., Estokova, A., Terpakova, E., Geffert, A., Kacik, F., et al. (2014). Properties characterization of chemically modified hemp hurds. Materials, 7(12), 8131-8150. https://doi.org/10.3390/ma7128131

[50] Carvalheiro, F., Silva-Fernandes, T., Duarte, L. C., & Gírio, F. M. (2009). Wheat straw autohydrolysis: Process optimization and products characterization. Applied Biochemistry and Biotechnology, 153(1-3), 84-93. https://doi.org/10.1007/s12010-008-8448-0

[51] Kabel, M. A., Bos, G., Zeevalking, J., Voragen, A. G. J., & Schols, H. A. (2007). Effect of pretreatment severity on xylan solubility and enzymatic breakdown of the remaining cellulose from wheat straw. Bioresource Technology, 98(10), 2034-2042. https://doi.org/10.1016/j.biortech.2006.08.006

[52] Sjostrom, E. (1993). Wood chemistry: Fundamentals and applications Gulf professional publishing. San Diego: Academic press. 292

[53] Miller, D. P., & Moslemi, A. A. (2007). Wood-cement composites: Effect of model compounds on hydration characteristics and tensile strength. Wood and Fiber Science, 23(4), 472-482.

[54] Soroushian, P., Aouadi, F., Chowdhury, H., Nossoni, A., & Sarwar, G. (2004). Cement-bonded straw board subjected to accelerated processing. Cement and Concrete Composites, 26(7), 797-802. https://doi.org/10.1016/j.cemconcomp.2003.06.001

[55] Hachmi, M., Moslemi, A. A., & Campbell, A. G. (1990). A new technique to classify the compatibility of wood with cement. Wood Science and Technology, 24(4), 345-354. https://doi.org/10.1007/bf00227055

[56] Alberto, M. M., Mougel, E., & Zoulalian, A. (2000). Compatibility of some tropical hardwoods species with portland cement using isothermal calorimetry. Forest Products Journal, 50(9), 83

[57] Jorge, F. C., Pereira, C., & Ferreira, J. (2004). Wood-cement composites: A review. Holz Als Roh-Und Werkstoff, 62(5), 370-377. https://doi.org/10.1007/s00107-004-0501-2

[58] Matoski, A., Hara, M. M., Iwakiri, S., & Casali, J. M. (2013). Influence of accelerating admixtures in wood-cement panels: Characteristics and properties. Acta Scientiarum. Technology, 35(4), 655-660. https://doi.org/10.4025/actascitechnol.v35i4.11261

[59] Abou Diab, A., Sadek, S., Najjar, S., & Abou Daya, M. H. (2016). Undrained shear strength characteristics of compacted clay reinforced with natural hemp fibers. International Journal of Geotechnical Engineering, 10(3), 263-270. https://doi.org/10.1080/19386362.2015.1132122

[60] Murphy, F., Pavia, S., & Walker, R. (2010). An assessment of the physical properties of lime-hemp concrete. Proceeding of the Bridge and Concrete Research in Ireland, Cork.

[61] Farooqila, M. U., & Ali, M. (2016). Compressive behavior of wheat straw reinforced concrete for pavement applications. Paper presented at the Proc. Fourth Int. Conf. on Sustainable Construction Materials and Technologies

[62] Sinka, M., Sahmenko, G., Korjakins, A., Radina, L., & Bajare, D. (2015). Hemp thermal insulation concrete with alternative binders, analysis of their thermal and mechanical

properties. Paper presented at the IOP Conference Series: Materials Science and Engineering, 96. (1) pp. 012029. https://doi.org/10.1088/1757-899x/96/1/012029

[63] Balčiūnas, G., Vėjelis, S., Vaitkus, S., & Kairytė, A. (2013). Physical properties and structure of composite made by using hemp hurds and different binding materials. Procedia Engineering, 57, 159-166. https://doi.org/10.1016/j.proeng.2013.04.023

[64] Shen, C. -H., & Springer, G. S. (1976). Moisture absorption and desorption of composite materials. Journal of Composite Materials, 10(1), 2-20. https://doi.org/10.1177/002199837601000101

[65] Mbou, E. T., Njeugna, E., Kemajou, A., Sikame, N. R., & Ndapeu, D. (2017). Modelling of the water absorption kinetics and determination of the water diffusion coefficient in the pith of Raffia vinifera of Bandjoun, Cameroon. Advances in Materials Science and Engineering, 2017, 1-12. https://doi.org/10.1155/2017/1953087

[66] Daniel, I. M., Ishai, O., Daniel, I. M., & Daniel, I. (2006). Engineering mechanics of composite materials Oxford university press New York.

[67] Hewlett, P., & Liska, M. (2019). Lea's chemistry of cement and concrete Butterworth-Heinemann.

[68] Glenn, G. M., Gray, G. M., Orts, W. J., & Wood, D. W. (1999). Starch-based lightweight concrete: Effect of starch source, processing method, and aggregate geometry. Industrial Crops and Products, 9(2), 133-144.

[69] Meza, A., & Siddique, S. (2019). Effect of aspect ratio and dosage on the flexural response of FRC with recycled fiber. Construction and Building Materials, 213, 286-291. doi:https://doi.org/10.1016/j.conbuildmat.2019.04.081

[70] Yoo, D., Kim, S., Park, G., Park, J., & Kim, S. (2017). Effects of fiber shape, aspect ratio, and volume fraction on flexural behavior of ultra-high-performance fiber-reinforced cement composites. Composite Structures, 174, 375-388. doi:https://doi.org/10.1016/j.compstruct.2017.04.069